Available online at www.sciencedirect.com
ScienceDirect
Icarus 190 (2007) 203–223
ICARUS
www.elsevier.com/locate/icarus

Can planetesimals left over from terrestrial planet formation produce the lunar Late Heavy Bombardment?

William F. Bottke *, Harold F. Levison, David Nesvorný, Luke Dones

Southwest Research Institute, 1050 Walnut St., Suite 400, Boulder, CO 80302, USA

Received 22 August 2006; revised 17 January 2007

Available online 12 March 2007

Abstract

The lunar Late Heavy Bombardment (LHB) defines a time between ~3.8 to possibly 4.1 Gy ago when the Nectarian and early-Imbrium basins on the Moon with reasonably well-constrained ages were formed. Some have argued that these basins were produced by a terminal cataclysm that caused a spike in the inner Solar System impactor flux during this interval. Others have suggested the basins were formed by the tail end of a monotonically decreasing impactor population originally produced by planet formation processes in the inner Solar System. Here we investigate whether this so-called declining bombardment scenario of the LHB is consistent with constraints provided by planet formation models as well as the inferred ages of Nectaris, Serenitatis, Imbrium, and Orientale. We did this by modeling the collisional and dynamical evolution of the post-planet formation population (PPP) for a range of starting PPP masses. Using a Monte Carlo code, we computed the probability that the aforementioned basins were created at various times after the Moon-forming event approximately 4.54 Ga. Our results indicate that the likelihood that the declining bombardment scenario produced Nectaris, Serenitatis, Imbrium, and Orientale (or even just Imbrium and Orientale) at any of their predicted ages is extremely low and can be ruled out at the 3σ confidence level, regardless of the PPP's starting mass. The reason is that collisional and dynamical evolution quickly depletes the PPP, leaving behind a paucity of large projectiles capable of producing the Moon's youngest basins between 3.8–4.1 Gy ago. If collisions are excluded from our model, we find that the PPP produces numerous South Pole-Aitken-like basins during the pre-Nectarian period. This is inconsistent with our understanding of lunar topography. Accordingly, our results lead us to conclude that the terminal cataclysm scenario is the only existing LHB paradigm at present that is both viable from a dynamical modeling perspective and consistent with existing constraints.

Keywords: Asteroids; Asteroids, dynamics; Collisional physics; Impact processes; Origin, Solar System

1. Introduction

The lunar Late Heavy Bombardment (LHB) describes a time ~3.8 to perhaps 4.1 Gy ago (hereafter Ga) when the basins with reasonably well-determined ages on the Moon were formed (see reviews in Hartmann et al., 1981, 2000; Ryder et al., 2000; Warren, 2004). This topic has been fraught with controversy ever since it was introduced by Tera et al. (1974) as a means to explain the absence of lunar rocks with isotopic recrystallization ages >4.0 Gy old. Nearly all lunar impact melt breccia samples have been found to have ages between 3.8 and 4.0 Gy old (e.g., Warren, 2004). Tera et al., argued this curious result was best explained by a terminal cataclysm that was a byproduct of a spike in the inner Solar System impactor flux between ~3.8–4.0 Ga. Over the last several decades, numerous geologic, cosmochemical, and dynamical arguments have been made in support of the terminal cataclysm model. A few of the more recent articles on this issue include Dalrymple and Ryder (1993), Ryder et al. (2000), Levison et al. (2001), Cohen et al. (2000), Kring and Cohen (2002), Chambers and Lissauer (2002), Gomes et al. (2005), Norman and Taylor (2005), Strom et al. (2005), Norman et al. (2006), Trail et al. (2007).

Others have argued that the LHB was actually the tail end of a monotonically decreasing impactor population originally produced by planet formation processes in the inner Solar System (e.g., Hartmann et al., 2000). We refer to this scenario as the declining bombardment. Support for this idea

* Corresponding author. Fax: +1 303 546 9687.
E-mail address: bottke@boulder.swri.edu (W.F. Bottke).

0019-1035/$ – see front matter
doi:10.1016/j.icarus.2007.02.010

and/or skepticism for the terminal cataclysm scenario is prominent in the lunar literature (e.g., Hartung, 1974; Hartmann, 1975; Neukum, 1977; Wetherill, 1977; Baldwin 1987a, 1987b, Grinspoon, 1989; Neukum and Ivanov, 1994; Haskin et al., 1998; Morbidelli et al., 2001; Hartmann, 2003; Warren, 2003; Baldwin, 2006; Chapman et al., 2007; see Hartmann et al., 2000 for a recent review). If true, the terminal cataclysm as described above did not take place, though the declining bombardment population may have occasionally produced spikes in the lunar impact record (Hartmann, 1980). Assuming the declining bombardment scenario is correct, the Moon and presumably the other terrestrial planets were subject to highly energetic impact events from ∼4.5 to ∼3.8 Ga. The paucity of >4.0 Ga lunar rocks would then be a byproduct of this bombardment, with the oldest lunar rocks continually obliterated and replaced by younger ones (Grinspoon, 1989; see also Hartmann et al., 2000).

Alternatively, these data could simply represent a sampling bias. Haskin et al. (1998) argued that the frontside of the Moon was blanketed by ejecta produced by the Imbrium basin-forming event at ≈3.85 Ga. If taken to an extreme, this could imply that nearly every ancient lunar sample from the Apollo and Luna collections, and perhaps most lunar meteorites as well, were somehow connected to the Imbrium impact. Recent work by Norman et al. (2006), however, is inconsistent with this hypothesis. Using modern techniques, they measured high resolution ^{40}Ar–^{39}Ar ages on Apollo 16 impact melt breccias found on the central nearside lunar highlands. Their results indicate that at least 4 prominent melt-producing impact events took place between 3.75 and 3.95 Ga. This implies that contamination from Imbrium is limited and the Moon was indeed on the receiving end of several distinct basin-forming events over this interval. The nature of this bombardment, however, is still in dispute.

The resolution of the LHB enigma is critical to our understanding of not only planet formation but also of how the Solar System reached its final configuration. The perennial problem is that the available information on the LHB from lunar data, collected by a wide variety of sources (e.g., the Apollo and Luna programs, ground-based observing programs, lunar meteorites, data from unmanned spacecraft, etc.), has led to ambiguous or conflicted conclusions from researchers in the field. In fact, some of the same lunar evidence has been used to support both the terminal cataclysm and the declining bombardment paradigms.

Regardless of how the LHB constraints are viewed, both camps, in the end, need a working dynamical model of their version of the LHB that is consistent with the most accurate lunar data (e.g., the formation of the large lunar basins Imbrium and Orientale between 3.9–3.7 Ga; see Section 2.3). Over the last several years, significant progress toward such a model has been made in the terminal cataclysm camp by Levison et al. (2001), Tsiganis et al. (2005), Morbidelli et al. (2005), and Gomes et al. (2005). We will describe these papers in greater detail in Section 2.1.

For the declining bombardment scenario, the best available dynamical model at present is that of Morbidelli et al. (2001). Using planet formation models, they showed that evolving planetary embryos in the terrestrial planet region are likely to scatter numerous planetesimals into long-lived high-inclination orbits. Accordingly, this population of planet formation leftovers might produce a slow-decaying bombardment on the Moon (and other terrestrial planets) lasting from the Moon's formation all the way to ∼3.8 Ga. To check this, Morbidelli et al. (2001) tracked the evolution of test bodies in this scenario for 100–300 My using initial conditions taken from planet formation simulations and then extrapolated those results to the LHB epoch. Overall, they found their model did a good job of reproducing the population of diameter $D_{\rm crater} > 10$ km craters found on the ancient lunar cratered terrains as described by Neukum and Ivanov (1994).

A reexamination of Morbidelli et al. (2001) by our team, however, indicates several key aspects of their model may require increased scrutiny. For example, Morbidelli et al. (2001) did not directly compare their results to those large lunar basins whose ages are reasonably well-constrained by lunar samples (though they did assert that their model would likely have difficulty reproducing the relatively young ages of basins with ∼3.8–3.9 Ga ages; see Section 2.3). As a second example, it is unclear whether tracking potential lunar projectiles for 100–300 My after the formation of the Moon is sufficiently long to characterize their dynamical behavior all the way to the LHB epoch and beyond. Note that the declining bombardment model must not only reproduce the large lunar basins with reasonable age constraints but must also explain why no basins are apparently younger than ∼3.8 Gy. Numerical integration runs that track a statistically significant number of test bodies beyond 600–800 My have yet to be attempted. Finally, insights gleaned from Bottke et al. (2005a, 2005b, 2006a) suggest that collisional evolution between members of the lunar impacting population could diminish the number of projectiles available to strike the Moon in the declining bombardment paradigm. Collisional grinding within the lunar impactor population has yet to be considered in the context of the LHB.

For these reasons, we decided to re-investigate the declining bombardment paradigm of the LHB. The outline of our paper is as follows. In Section 2, we provide additional background on the terminal cataclysm and declining bombardment models of the LHB while also discussing the constraints provided by the lunar basins whose ages are known to reasonable precision. In Section 3, we describe our initial conditions as well as the numerical procedure used to simulate the evolution of the *post-planet formation population*, which we define in this paper as the PPP. In Section 4, we compute the dynamical decay rate of the PPP as well as the impact rate it has with the Moon. We then use this information to estimate the size of the initial PPP and discuss whether it is consistent with existing planet formation models. We then allow the PPP to undergo collisional evolution as well as dynamical depletion and discuss how these processes affect our estimate of the initial PPP. Finally, Section 5 contains our conclusions and some discussion of the implications of this work for the timing of events occurring on the terrestrial planets early in Solar System history. As an aside, Appendix A examines several niches in semimajor axis a, eccentricity e, and

inclination i space where test bodies from our numerical integration work were found to have considerably longer dynamical lifetimes than those of typical near-Earth objects (NEOs).

2. Background on modeling the lunar Late Heavy Bombardment

2.1. A dynamical model for the terminal cataclysm paradigm

Before focusing our attention on the declining bombardment, we believe it is useful to first describe how its main competitor explains the LHB. Recent dynamical modeling work by Tsiganis et al. (2005), Morbidelli et al. (2005), and Gomes et al. (2005) indicates that a plausible scenario may now exist to not only reproduce the terminal cataclysm but also explain many other longstanding problems in Solar System dynamics. These papers are commonly referred to as the "Nice" model, named after the Observatoire de la Côte d'Azur in Nice, France where it was developed. For reference, these papers were built on many of the ideas contained in Wetherill (1975), Levison et al. (2001), and Levison et al. (2004).

In the Nice model, the jovian planets were assumed to have grown on initially nearly circular, coplanar orbits with a more compact configuration than they have today (all were located between 5–15 AU). Slow planetary migration was induced in the jovian planets by gravitational interactions with planetesimals leaking out of a $\sim 35 M_{\oplus}$ planetesimal disk residing between $\sim$16 to $\sim$30 AU. These interactions steadily stretched the system of planets over hundreds of My. Eventually, after a delay of $\sim$600 My set by the initial configuration of the gas giants (Gomes et al., 2005), Jupiter and Saturn crossed their mutual 1:2 mean motion resonance, which caused their e and i values to jump from values near zero to their current values. In turn, this caused Uranus and Neptune to become unstable and be scattered outward, such that they penetrated the disk and migrated through it. The orbits of Uranus and Neptune were then circularized by dynamical friction produced by bodies in the disk. As described by Tsiganis et al. (2005), this model does a good job of reproducing the orbital parameters (a, e, i) of the jovian planets. Moreover, scattered planetesimals captured during the LHB into Jupiter Trojan orbits (i.e., orbits around Jupiter's Lagrangian L_4 and L_5 points) had i values that are consistent with those of the observed population (Morbidelli et al., 2005). This potentially solves a long-standing problem in understanding the formation of those bodies (e.g., Marzari et al., 2002).

With Jupiter and Saturn shifting to new orbits, inner Solar System resonances like the ν_6 and ν_{16} secular resonances moved to new locations (Gomes et al., 2005). Numerical simulations suggest they may have swept across the main belt region. In the process, they would have ejected numerous asteroids from that stable zone. Thus, the Nice model predicts that the terminal cataclysm may be a combination of cometary bodies scattered by Uranus/Neptune and asteroids pushed out of the main belt.

Gomes et al. (2005) predicted the instability in the Nice model should have significantly increased the inner Solar System small body population near 3.9 Gy. Their estimates indicate that material ejected from the main belt alone could have caused the Earth/Moon-crossing populations to grow by 3–4 orders of magnitude over their present-day populations for a timescale lasting tens of My to perhaps 100–200 My. 1–10 times the current main belt population. The size of this predicted bombardment appears to be consistent with the mass accreted by the Moon during the LHB (see also Levison et al., 2001). It is also interesting to note that the impact signature produced by the LHB on the Moon is consistent with the current shape of the main belt size distribution (Strom et al., 1992, 2005; A. Cheng, personal communication) as well as its predicted shape 3.8–3.9 Ga (Bottke et al., 2005a, 2005b).

There are still several issues related to the Nice terminal cataclysm model that could be better quantified. For example, it is not known whether the LHB impactors in the Nice model were mostly asteroids, mostly comets, or some roughly equal combination of the two. Note that while Strom et al. (2005) predicted that the crater size distribution found on the lunar highlands was consistent with impactors from the main belt, this might only tell us that the asteroidal component of the LHB struck after the cometary component (Gomes et al., 2005). The true shape of the cometary size distribution at the time of the LHB (and now) is unknown (Bernstein et al., 2004); if the scaling laws controlling comet breakup events are similar to those of asteroids, and collisional grinding within the disk of objects beyond 15 AU was significant between 4.5–3.9 Gy ago, it is conceivable that the main asteroid belt and cometary source size distributions had similar shapes (O'Brien et al., 2005; see also Bottke et al., 2005a, 2005b). On the other hand, Kring and Cohen (2002) used the siderophile element signatures in lunar impact melt samples to argue that the projectiles that formed the major nearside basins could not have had comet-like compositions (see also Tagle, 2005). The debate on this issue will likely continue until additional samples are returned from the Moon.

The terminal cataclysm model of the LHB has recently gained support from studies of Hadean-era zircons on Earth (Trail et al., 2007). These ancient objects, which formed prior to the LHB, show a sequence of secondary overgrowths that may have been formed by shock heating and metamorphism events produced by enormous terrestrial impacts $\sim$3.9 Gy ago. Trail et al., argue that the lack of comparable features in pre-Archean zircons implies that the LHB was most likely a terminal cataclysm rather than a declining bombardment.

While there are clearly aspects of the Nice model that need to be better understood, this work has raised the bar for other LHB models. For this reason, we believe it is of critical importance to evaluate the declining bombardment scenario. The rest of the paper will concentrate on this topic.

2.2. A dynamical model for the declining bombardment paradigm

In order to probe the declining bombardment paradigm and the nature of the putative post-planet formation population

(PPP), it is useful to first briefly review what is known about the primordial population of planetesimals that make up the inner Solar System planets. The history of small bodies in the inner Solar System begins when dust-sized bodies form out of the Solar Nebula. These dust motes eventually grow into km-sized planetesimals through inelastic collisions between particles (e.g., Weidenschilling, 2003) or gravitational instabilities (e.g., Goldreich and Ward, 1973; Youdin and Chiang, 2004; Tanga et al., 2004; Youdin and Goodman, 2005). At this point, objects in distinct feeding zones undergo runaway growth, allowing numerous protoplanets to emerge from the swarm of material that surrounds them (e.g., Greenberg et al., 1978; Wetherill and Stewart, 1989; Weidenschilling et al., 1997; Kokubo and Ida, 2002). This leaves most of the system's mass concentrated in a relatively small number of bodies. Chaotic interactions between the protoplanets eventually lead to mergers and the formation of the terrestrial planets over a timescale of several tens of My (e.g., Wetherill, 1992; Weidenschilling et al., 1997; Chambers and Wetherill, 1998; Agnor et al., 1999; Chambers, 2001; Chambers and Wetherill, 2001; Chambers and Cassen, 2002; Petit et al., 2001; Levison and Agnor, 2003; Raymond et al., 2004; 2006; McNeil et al., 2005; Kenyon and Bromley, 2006; Kokubo et al., 2006; O'Brien et al., 2006; Chambers, 2006). At the same time, gravitational perturbations from the embryos dynamically excited the leftover planetesimals to high inclinations. This prevented many of them from agglomerating with the new planets.

We define the PPP to be the inner Solar System planetesimal population that existed after the Moon was formed. The best available evidence indicates the lunar forming impact occurred near the very end of Earth's accretion some 30 My after the formation of the first solids in the Solar System (see Canup, 2004, for a recent review). There are several possible endstates for objects in the PPP. Some strike one another at high velocities and disrupt. Others strike the Sun or are scattered out of the inner Solar System by gravitational interactions with the planets. While a few go on to strike the newly-formed Moon and terrestrial planets, the remainder stay in the inner Solar System and, by necessity, are driven into regions of (a, e, i) space where the timescales for their removal are long.

The dynamical evolution of the PPP was most recently examined by Morbidelli et al. (2001) (an earlier treatment of this problem can be found in Wetherill, 1977). Using late stage planet formation simulations by Chambers and Wetherill (1998), Morbidelli et al. (2001) generated initial conditions for different PPPs and tracked the dynamical evolution of test bodies on these orbits for at least 100 My. Overall, Morbidelli et al. (2001) found the median dynamical lifetime of PPP bodies was 50–60 My with a decay rate proportional to $e^{-t/77}$ (time t in My). Next, using established codes (e.g., Farinella and Davis, 1992), they computed the collision probabilities and impact velocities between their PPP and the Moon in order to compare their results with LHB constraints. Their work focused on data provided by Neukum and Ivanov (1994), who estimated that the number of $D > 10$ km craters formed on the Moon between 4.4–3.9 Ga was 10^{-3} per square km or 40,000 craters when integrated over the entire surface. Morbidelli et al. (2001) found their numerical results for the declining bombardment were consistent with these data. It is important to point out, however, that the most ancient craters on the lunar highlands are in saturation equilibrium; this would make the Neukum and Ivanov values lower limits on the total number of craters formed.

Morbidelli et al. (2001) also compared their results to the number of basins formed on the Moon prior to 3.9 Ga, where a basin was defined as a crater with diameter $D_{\rm crater} > 300$ km. For this test, they assumed that the 28–45 basins tabulated by Wilhelms (1987) were formed between 4.4–3.9 Ga and that they comprised a complete set. No specific age information was assumed for any particular basin. The 4 largest lunar basins were assumed to have formed by $D > 50$ km projectiles over the same time span. Their work suggested they could reproduce this basin population if their initial PPP contained ∼10,000 bodies larger than $D > 20$ km and 1000 bodies larger than $D > 50$ km. These values are approximately 5 and 2 times the current main belt population, respectively.

While the Morbidelli et al. (2001) declining bombardment model has many positive attributes, our reexamination of their work indicates some of their assumptions and results may be problematic:

- The Morbidelli et al. (2001) declining bombardment model predicts that almost all of the large lunar basins should have formed early in the 4.5–3.8 Ga epoch. As will be described in Section 2.3, however, several prominent lunar basins with reasonably constrained ages formed at the end of this time period. This was recognized by Morbidelli et al. (2001) to be at odds with their model results and was specifically cited in their paper as a potentially serious problem for their model. They also assumed that the $D > 10$ km craters discussed by Neukum and Ivanov (1994) formed between 4.4–3.9 Ga. The ages of these craters, however, are model dependent; they could have also have formed during the terminal cataclysm. Without additional age information, these small craters cannot be used to differentiate between the terminal cataclysm and declining bombardment models of the LHB.
- They assumed that their test body runs, which only went 100–300 My after planet formation, could be extrapolated to ∼600 My or beyond. This approximation may be reasonable, but it has yet to be confirmed by numerical simulations. Moreover, it prevented them from examining whether their declining bombardment model produced any basins younger than 3.8 Ga (see Section 2.3).
- They assumed that the PPP experienced little collisional evolution over its lifetime. Given the size of the PPP and the high collision probabilities and impact velocities of PPP objects with one another, however, we believe this approximation is invalid and in fact may prevent the PPP from matching the constraints of the LHB.

In Sections 3–4, we will critically reexamine these assumptions and determine whether they are consistent with existing LHB constraints.

2.3. Constraints on lunar basin formation

In order to constrain the LHB, we need to first understand, as best as possible with the available data, the early impact history of the Moon. Since the time of the Apollo program, it has been known that the Moon experienced an extraordinarily intense bombardment of comets and/or asteroids some time between ~4.5 and 3.8 Ga. While the duration, intensity, and nature of the impact flux over this timespan is still being debated, it is agreed that the largest and most prominent lunar impact features were created during this interval. Wilhelms (1987) claims that at least 40 basins were produced on the Moon with ages >3.8 Ga (see also Cook et al., 2000). Some notable examples include the South-Pole Aitken basin ($D_{\text{crater}} \sim 2600$ km), the Imbrium basin ($D_{\text{crater}} \sim 1160$ km), and the Orientale basin ($D_{\text{crater}} \sim 930$ km) (a compilation of basin data can be found at the Impact Basin Database; Wood, 2004).

The production of more than 40 basins on the Moon over a ~700 My time period (or less) represents at least a 2–3 orders of magnitude increase in the impactor flux over the current flux (e.g., Wilhelms, 1987). For reference, the post-mare cratering rate on the Moon over the last 3 Gy has been $\sim 3 \times 10^{-15}$ km^{-2} yr^{-1} for $D_{\text{crater}} \geqslant 20$ km (e.g., Grieve and Shoemaker, 1994; Shoemaker and Shoemaker, 1996; McEwen et al., 1997; Shoemaker, 1998; see also Bottke et al., 2005a, 2005b). The largest impact structure formed on the Moon during the last ~3 Gy is Langrenus, a 132 km crater that is too small to qualify for basin status (McEwen et al., 1993). We infer from this data that the early impact history of the Moon was very different from that of the last few Gy.

The ages of some of the lunar basins described above have been inferred from an analysis of (i) lunar samples collected by the Apollo and Luna programs (e.g., crystallization ages of rock units, ages of impact melts, degree of crustal contamination by meteoritic material), (ii) geologic investigations of the stratigraphy and degree of degradation of observed basins, and (iii) crater counts and the superposition of basins and craters. Using this information as a guide, Wilhelms (1987) divided lunar history prior to the formation of the Orientale basin, the youngest multi-ring basin on the Moon (3.84–3.72 Ga; Stöffler and Ryder, 2001), into 3 phases: pre-Nectarian, Nectarian, and early-Imbrium. For the Nectarian and early-Imbrium periods, Wilhelms (1987) assumed the deposits of the Nectaris and Imbrium basins defined the pre-Nectarian/Nectarian and Nectaris/Imbrium boundaries. We discuss each period below.

2.3.1. Pre-Nectarian period

The pre-Nectarian period represents the earliest observable phase of lunar history. Much of its terrain is located on the far side of the Moon. Wilhelms (1987) identified 30 multi-ring basins and/or their ejecta formed during this epoch, including the South Pole-Aitken basin and Procellarum, the latter of which may not be an impact basin (Smith et al., 1997). Digital elevation models and stereoimagery of the Moon have recently increased this number to 36 (Cook et al., 2000). Unfortunately, not only do most of these basins have indeterminate ages, but the starting time of the pre-Nectarian period is poorly understood. For example, some argue this period extends all the way back to the oldest recorded lunar material (4.52 Ga; Lee et al., 1997; Halliday, 2000), while others claim that the oldest pre-Nectarian basins formed between 4.2–4.1 Ga (Wilhelms, 1987) or even 3.9 Ga (e.g., Stöffler and Ryder, 2001).

Another problem with interpreting the record of pre-Nectarian basins is that they may be incomplete. It is likely that at least a few ancient basins have been covered up or obliterated by impact events occurring later in lunar history. It is also conceivable that the lunar surface was, at some time in the distant past, saturated with basins (C. Chapman, personal communication). If true, a significant portion of the Moon's early history could have been erased.

With this said, saturated lunar terrains cannot hide endless numbers of giant basins without leaving behind some traces (e.g., Norman and Taylor, 2005). As an example, consider South Pole-Aitken, the largest undisputed basin on the Moon with $D_{\text{crater}} = 2600$ km. Zahnle and Sleep (1997) estimate the energy needed to form South Pole-Aitken was roughly 1×10^{34} ergs, give or take a factor of 4. Topographic maps on the Moon from the Clementine spacecraft show South Pole-Aitken to be an easily recognizable, singular feature that is 12 km lower than the surrounding highlands (Smith et al., 1997; Cook et al., 2000). The only comparable feature in the inner Solar System is the Chryse Basin on Mars (Taylor, 1998). If additional South Pole-Aitken-like basins had formed on the Moon in the pre-Nectarian period, they would have presumably left behind deep scars that would readily show up on a lunar topographic map. The fact that we have yet to find evidence for such deep holes nor lunar mantle material excavated by big impacts implies that the South Pole-Aitken basin may have been the largest impact event on the Moon since the formation of its crust. Analysis of a ferroan noritic anorthosite clast from a lunar breccia indicates that lunar crust formation on the Moon occurred at 4.46 ± 0.04 Gy, roughly 100 My after the formation of the earliest datable solids found in primitive meteorites (Norman et al., 2003). This value, if accurate, places an important limit on the nature of the population striking the Moon between 4.46 Ga and today.

2.3.2. Nectarian period

The boundary of the pre-Nectarian/Nectarian period is marked by the formation of the Nectaris basin ($D_{\text{crater}} = 860$ km). The age of this basin is controversial. Using photogeologic methods and stratigraphy alone, Nectaris appears to be older than Imbrium and Serenitatis (Wilhelms, 1987; Baldwin, 2006). The most frequently cited age for Nectaris, based on an analysis of ^{40}Ar–^{39}Ar ages from Apollo 16 impact clasts, is 3.92 Ga, though some prefer an age as young as 3.85 Ga [see Stöffler and Ryder (2001) and Warren (2004) for recent reviews]. The detection of 4 large impact events in the Apollo 16 data between 3.75–3.95 Ga by Norman et al. (2006) provides some evidence, albeit circumstantial, that these ages are reasonable. On the other hand, others have argued that at least some Apollo 16 samples are ejecta from the Imbrium impact, and that the true Nectaris age is 4.12 Ga (Korotev et al., 2002; Warren, 2003).

The ambiguous age of Nectaris has allowed it to be cited as evidence both for and against the terminal cataclysm scenario (Hartmann et al., 2000). By superposition arguments, a young Nectaris pushes some basin formation events toward ages younger than 3.9 Ga. This provides support to those who argue that the LHB was a cataclysm rather than a declining bombardment. Alternatively, an older Nectaris lends credence to the idea that basin-forming impacts took place on the Moon over most of its early history.

Observations indicate 12 multi-ring basins were formed in the Nectarian period (i.e., defined as the age sequence between the formation of the Nectaris and Imbrium basins; Wilhelms, 1987). A few of these basins have reasonably precise age estimates (e.g., Crisium, a $D_{\text{crater}} = 740$ km crater formed 3.84–3.89 Ga; Serenitatis, a $D_{\text{crater}} = 920$ km crater formed 3.893–3.87 Ga; see Stöffler and Ryder, 2001). The age estimate of Serenitatis may have been affected by Imbrium ejecta (Haskin et al., 1998). Using photogeologic arguments alone, however, Wilhelms (1987) and Baldwin (2006) claim that Serenitatis formed after Crisium but before Imbrium.

2.3.3. Early-Imbrium period

The formation of the Imbrium basin marks the end of the Nectarian and the beginning of the early-Imbrium period. Depending on the samples used, Imbrium has several possible ages. According to materials returned by the Apollo program, Imbrium has an estimated age of 3.85 ± 0.02 or 3.77 ± 0.02 Ga (Stöffler and Ryder, 2001). On the other hand, using the lunar meteorite Sayh al Uhaymir, Gnos et al. (2004) estimated Imbrium's age to be 3.909 ± 0.013 Ga. The early-Imbrium period terminates with the formation of the Orientale basin, which may be 3.84–3.72 Gy old (Stöffler and Ryder, 2001). The younger constraint is set by the oldest age of nearby exposed mare basalts of Upper Imbrium age produced after Orientale (Wilhelms, 1987). The consensus opinion based on crater counts and photogeology is that the Imbrium and Orientale basins formed close in time to one another and marked the end of large basin-formation events on the Moon (Wilhelms, 1987; Baldwin, 2006).

2.3.4. Summary of constraints

Given this information, we conclude that the largest Nectarian and early-Imbrium basins provide the best constraints for our LHB model results. The early-Imbrium basins are of particular importance because there is relatively little debate over their absolute ages; they simply do not suffer from the same age ambiguities that afflict the other lunar basins. *As we will show, this means the very existence of Imbrium and Orientale themselves may be enough to rule out the declining bombardment scenario.*

In order to give the declining bombardment scenario as fair an opportunity as possible, we assumed the Nectarian and early-Imbrium basins formed over a wide range of ages, with the Nectarian period beginning 4.12 or 3.92 Ga, the early-Imbrium period beginning 3.91 or 3.85 Ga, and the early-Imbrium ending 3.82 or 3.72 Ga (Table 1). These ages are used below as mileposts to test whether the Nectarian and early-Imbrium basins were formed by the PPP. The four largest basins formed in the Nectarian and early-Imbrium periods, in order of decreasing size, were Imbrium, Orientale, Serenitatis, and Nectaris (1160, 930, 920, and 860 km, respectively). The two largest basins formed in the early-Imbrium period were Imbrium and Orientale.

Zahnle and Sleep (1997) estimate the energy needed to form Imbrium and Orientale were $1–3 \times 10^{33}$ and 1×10^{33} ergs, respectively. Given that Orientale, Serenitatis, and Nectaris all have similar-sized multi-ring structures (see Wood, 2004), we assume here that all were formed with roughly the same amount of impact energy. To be conservative in favor of the declining bombardment scenario, the lower end of this energy range is used in our modeling work.

The remaining ~12 basins of the Nectarian and early-Imbrium periods were produced by considerably lower energy impacts than the largest basins (e.g., $1–4 \times 10^{31}$ ergs or less) (Levison et al., 2001). While these smaller basins can also be used to tell us about the LHB, we are unsure whether they comprise a complete set. For example, several putative basins with unknown ages have been classified as "uncertain" or "proposed" at the Impact Basin Database (Wood, 2004). This means they lack central depressions, surrounding ejecta deposits, or multiple rings. In a few cases, the only evidence for their existence may come from circular depressions observed in Clementine altimetry data. This leads us to believe that an unknown number of small basins were obliterated by subsequent basin/cratering events and/or the emplacement of mare basalts. As such, we choose not to use them as constraints in this paper.

The LHB constraints used in our modeling work below are summarized here:

1. We assume that the starting time for the PPP ($t = 0\ My$) was the Moon-forming event that took place 4541 Ma, 30

Table 1
The approximate starting and ending times for the lunar time-stratigraphic units discussed in this paper

Lunar period	Start (Ga)	Start (t after MFE in My)	End (Ga)	End (t after MFE in My)
Pre-Nectarian	Unknown	Unknown	4.12 or 3.92	421 or 621
Nectarian	4.12 or 3.92	421 or 621	3.91 or 3.85	631 or 691
Early Imbrium	3.91 or 3.85	631 or 691	3.82 or 3.72	721 or 821

The third and fifth columns provide the same information in an alternative manner. Here elapsed time is measured after the Moon-forming event (MFE) at $t = 0$ My. For reference, we assume the MFE occurred 4.541 Ga. Our model constraints are as follows. Basin set A assumes Nectaris, Serenitatis, Imbrium, and Orientale formed in the Nectarian and early-Imbrium periods. Basin set B assumes Imbrium and Orientale formed in the early-Imbrium period.

My after the formation of the first solids 4571 Ma (Kleine et al., 2002; Shukolyukov and Lugmair, 2002). Here t is defined as the time after the Moon formed. The use of significant figures here does not imply degree of accuracy; rather it is included for mathematical convenience in our modeling work.

2. The approximate ages of the large basins described above are used as constraints in the LHB models described below. Given uncertainties about the age of Nectaris as well as the possible contamination of both Nectaris and Serenitatis by Imbrium ejecta, we are careful to use two sets of basin ages to test our model results. For *basin set A*, we use the four largest Nectarian and early-Imbrium basins that may have formed over intervals of (using point 1, from shortest to longest): $t = 621$–721 My, 621–821 My, 421–721 My, and 421–821 My (Table 1). For *basin set B*, we confine ourselves to Imbrium and Orientale, whose ages are reasonably well-dated. We assume they formed over intervals of $t = 691$–721 My, 631–721 My, 691–821 My, and 631–821 My (Table 1).
3. No $D_{\text{crater}} > 900$ km basins have formed on the Moon since the end of the early-Imbrium period. This is a less restrictive version of the observation that no $D_{\text{crater}} > 300$ km basins can be found on terrains younger than the early-Imbrium period. Given the robust nature of our conclusions, we decided it was unnecessary to adopt the latter constraint in our paper, though it can readily be applied to future modeling work if needed.

We can also test our results against the reality check described below. While interesting, we believe point #4 should not yet be considered as quantitative or diagnostic as the above constraints until more is understood about the pre-Nectarian history of the Moon.

4. The impact event that created the South Pole-Aitken basin took place in the pre-Nectarian period, defined here as the time period between the solidification of the lunar crust, presumed to be 4.46 ± 0.04 Ga (Norman et al., 2003), and the formation of the Nectaris basin (see above). Given the large depth and diameter of South Pole-Aitken, we believe it is unlikely that many similar-sized basins were produced and erased during the pre-Nectarian. Thus, any LHB model that creates large numbers of South Pole-Aitken-like basins in the pre-Nectarian should be treated with skepticism.

3. Numerical methods

In this section, we track the dynamical evolution of bodies in the PPP residing in the terrestrial planet region. Our procedure is as follows. First, we define the initial conditions of the PPP (Section 3.1). Next, we numerically integrate the test bodies in our PPP for over 1 Gy of simulation time, following the procedure described in Section 3.2. The goal is to produce output that can be used in Section 4 to determine the decay and lunar impact rate of the PPP over time.

3.1. Initial conditions for the post-planet formation population

Our first task is to establish initial conditions for the PPP. This is challenging to do with precision because current planet formation models capable of tracking planetesimal evolution are unable as of yet to reproduce the orbital parameters (a, e, i) and sizes of Mercury, Venus, Earth, and Mars (e.g., Wetherill, 1992; Weidenschilling et al., 1997; Chambers and Wetherill, 1998; Agnor et al., 1999; Chambers and Wetherill, 2001; Chambers and Cassen, 2002; Petit et al., 2001; Raymond et al., 2004, 2006; Kenyon and Bromley, 2006; Kokubo et al., 2006; O'Brien et al., 2006). This problem may be solved in the near future by the inclusion of computationally-expensive physical processes such as gravitational interactions between planetary embryos and a massive disk of planetesimals that produces dynamical friction (Levison et al., 2005) and those between solid bodies and the remnant gas nebula that produces gas drag and embryo migration (Agnor and Ward, 2002; Kominami and Ida, 2004; McNeil et al., 2005; Kominami et al., 2005). Until that time, however, all researchers wanting to explore the PPP are forced to make certain compromises.

For example, Morbidelli et al. (2001) chose to investigate the PPP by tracking the evolution of test bodies started between 1–2 AU within the late stage planet formation simulations described by Chambers and Wetherill (1998). They found that interactions with Moon- to Mars-sized embryos drove a small fraction of the test bodies to high inclinations. In fact, the $a < 2$ AU bodies that survived 100 My generally had $i > 39°$. The planets responsible for driving their test bodies to these orbits, however, are only vaguely similar to our terrestrial planets; in many cases, they consisted of two planets comparable in size to Earth/Venus with eccentricities and inclinations reaching >0.1 and $>10°$, respectively. While we agree with the conclusions of Morbidelli et al. (2001) that the long-lived survivors of the PPP are likely to have high inclinations, the somewhat extreme orbits of their terrestrial planets may have driven their PPP to higher inclinations than would be expected from a more dynamically quiescent planetary population. This means that some particles may fill niches of orbital parameter space unobtainable by real objects.

To avoid this potential problem while still exploiting the insights gleaned from the Morbidelli et al. (2001) simulations, we selected test bodies for our PPP that had the same orbital parameters as the observed near-Earth objects (NEOs) with $a < 2$ AU and $i > 40°$. We found that 83 of the 2400 known NEOs with $a < 4$ AU (as of September 2003) matched this criterion. Their (a, e, i) orbits, which are shown in Fig. 1, are similar to the "Model 2" PPP from Morbidelli et al. (2001); the main difference is that the NEOs used here contain fewer objects with extreme inclinations ($i > 60°$). According to the numerical integration results from Bottke et al. (2002), who tracked the evolution of numerous test bodies from the main belt to the NEO region and beyond, these bodies have longer survival times than most NEOs. Thus, if there is some problem with our PPP initial conditions, we believe it would be one that favors longer rather than shorter dynamical lifetimes. As shown in Section 4.1, our results provide a reasonable match to an ex-

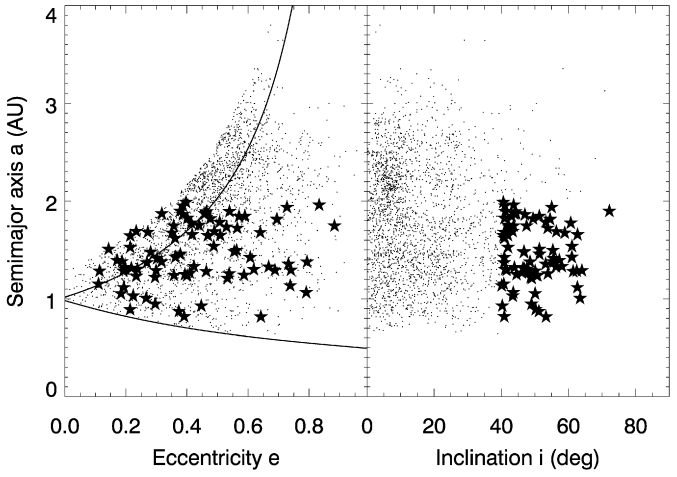

Fig. 1. The 2400 objects of the known near-Earth object (NEO) population with $a < 4$ AU as of September 2003. The 83 objects with semimajor axis $a < 2$ AU and inclination $i > 40°$ are shown as stars on the plot. These objects were chosen as starting conditions for our post-planet formation population (PPP). Those NEOs located between the solid lines in (a, e) space are on Earth and Moon-crossing orbits. Objects with perihelion $q \leqslant 1.017$ AU and aphelion $Q \geqslant 0.983$ AU fit this criterion.

trapolation of the Morbidelli et al. (2001) results for the basin formation times examined here ($t = 421$–821 Gy).

To better understand why high inclination NEOs have low loss rates (and why we use them as initial conditions for our PPP), it is useful to examine dynamical lifetimes among the entire NEO population. Bottke et al. (2002) found that most NEOs on $a > 2$ AU orbits only last a few My (at best), while those on $a < 2$ AU orbits may last as long as several tens to hundreds of My. NEOs with $a > 2$ AU have short lifetimes because the $2 < a < 3.5$ AU region is crisscrossed by powerful resonances (e.g., the 3:1, 5:2, and 2:1 mean motion resonances with Jupiter; the ν_6 secular resonance) and overlapping weaker resonances produced by Mars and other planets. The gravitational perturbations produced by these resonances, when combined with the orbit-changing effects of planetary encounters, readily push $a > 2$ AU NEOs onto orbits that allow them to strike the Sun or be readily ejected from the inner Solar System by encounters with Jupiter. The resonances located in the $a < 2$ AU region are weak by comparison (Michel, 1998; Michel et al., 2000). This means that objects achieving $a < 2$ AU orbits may wander the inner Solar System for an extended time before they strike a terrestrial planet or are pushed back onto an orbit with $a > 2$ AU. The time to reach $a > 2$ AU can be even longer for high inclination NEOs, in large part because their relative velocities with the terrestrial planets prevent close encounters from significantly modifying their orbits.

3.2. Numerical methods for tracking the evolution of the post-planet formation population

Numerical simulations completed on thousands of test NEOs to date have yet to identify any that can survive 600–800 My in the inner Solar System (i.e., the time from the Moon-forming event to the presumed end of the basin-forming era; Table 1). This does not mean that such long-lived objects do not or cannot exist, but rather that the runs completed to date have inadequate statistics to properly measure the long-lived tail of the NEO population.

There are two ways to directly determine the fraction of the population that can survive 600–800 My. The first is to track millions upon millions of test bodies until they are removed from the inner Solar System. While simple, this method requires far more CPU power than our team has available to it. The second way, which we adopt here, is to follow limited numbers of test bodies until some arbitrary fraction of the population has been removed from the system. The survivors are then cloned and the simulation continued until they are reduced by the same arbitrary fraction. This procedure is repeated until some test bodies reach 600–800 My after the start of the simulation. Ideally, the derived test body decay curve should be similar to that of the first method, provided the survivors circulate far enough within the inner Solar System to encounter all reachable (a, e, i) regions. Particles finding their way into local zones of stability within this space will live longer and thus will be more likely to be cloned at the end of each run. Over time, the lifetimes of these bodies should dominate the decay rate of the ensemble. Our goal is to determine the fraction of the PPP that survives long enough to produce the Nectarian and early-Imbrium basins via a declining bombardment.

The dynamical evolution of our PPP was computed using `swift_rmvs3`, a numerical integrator written by Levison and Duncan (1994) that was based on a symplectic algorithm published by Wisdom and Holman (1991). The gravitational perturbations of planets Venus through Neptune on their current orbits were included. The effect of Yarkovsky thermal drag on the PPP (e.g., Bottke et al., 2006b) was neglected because dynamics in NEO space for km-sized asteroids is dominated by planetary encounters and powerful resonances (Gladman et al., 1997; Migliorini et al., 1998; Bottke et al., 2000, 2002, 2006b). Test asteroids were tracked until they collided with the Sun, a planet, or were thrown beyond 6 AU from the Sun (usually by a close encounter with Jupiter). The timestep for our integrations was chosen to be 15 days.

To improve the statistics of our PPP, we cloned the 83 NEOs described above (Fig. 1) 16 times by giving them slight displacements to their orbital velocity vectors (10^{-6} AU yr^{-1}). (Note that because the Lyapunov times for our objects are typically shorter than 1000 years, even tiny velocity displacements to the starting conditions of our clones allow them to orbitally diverge on short timescales). We then sub-divided the 1328 particles into 8 groups of 166 particles apiece so they could run on eight processors devoted to long-term integrations. For reference, we define a *test case* as a run started on an individual processor. The orbits of the particles and their loss rate were output every 10,000 years. When the initial population from each test case was reduced to 12 particles, we cloned the remaining particles 10 times (for a total of 120 particles) and restarted the integrations. This will be referred to below as a *generation*. Each test case, made up of multiple generations, was followed for at least 1 Gy. In two test cases, we followed the clones all the way to ∼4 Gy.

4. Results

Here we use the results from the previous section to compute whether the PPP can produce the lunar basins with known ages (Section 2.3). Our procedure is as follows. First, we calculated the decay rate of our PPP as well as its normalized impact rate with the Moon (Sections 4.1–4.2). In this case, the initial size-frequency distribution of the PPP was treated as a free parameter. Next, we chose a shape for the PPP size distribution and used a Monte Carlo code to determine how big the initial PPP had to be to statistically produce the largest Nectarian and Early-Imbrium basins within various time intervals (Section 4.3). Finally, we explored how collisional evolution within the PPP affected the number of basin-forming projectiles available to strike the Moon during the LHB, with the results again tested using a Monte Carlo code (Section 4.4).

4.1. Dynamical decay rates for the post-planet formation population

An example of a six generation single test case is shown in Fig. 2. The fraction leaving the simulation has been scaled to properly account for loss rates among different generations, such that Fig. 2 shows the decay rate of the initial PPP vs time. The basin formation times are given in Table 1.

The time needed to reduce the first generation to 12 particles out of 166 (7%) was ≈ 60 My. The second generation particles had longer dynamical lifetimes than the first generation because many of the cloned survivors found zones of relative stability in the inner Solar System. In all, these bodies took ≈ 270 My to reach the 10% level (12 out of 120). Starting with the third generation, particle lifetimes began to follow a linear trend in log–log space, with the decay times growing steadily longer as the survivors in each generation find and/or reside within regions with long dynamical lifetimes. A line fit to the results in log–log space between the beginning of the third generation at 276 My and the end of the simulation at 4.34 Gy yields $\log_{10} f_{\rm left}(t) = 5.69 - 3.15 \log_{10} t$, where $f_{\rm left}(t)$ is the fraction of the population remaining in the simulation and t is the elapsed time in My. By extrapolating these results from this particular test run to 4.6 Gy, we estimate that $\sim 1 \times 10^{-6}$ of the original PPP population should be left in the inner Solar System region. In other words, the PPP survivors in this purely dynamical test case are literally one in a million. These results indicate there are indeed some zones of relative stability in the inner Solar System. Their (a, e, i) location will be discussed in Appendix A.

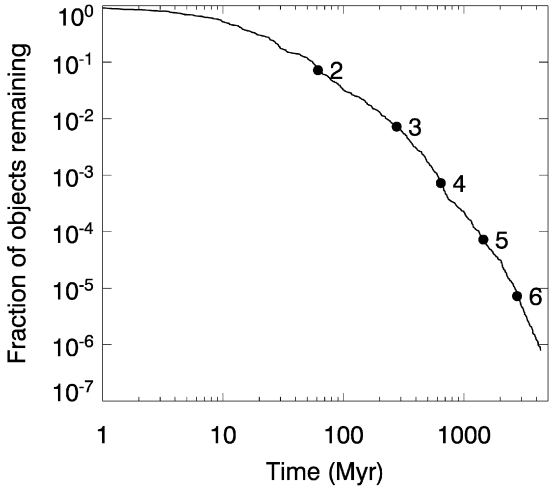

Fig. 2. The decay rate for a PPP test run started on a single processor. This initial test run contained 166 particles; two sets of 83 bodies with (a, e, i) orbits very similar to those described in Fig. 1. When this PPP was reduced to 12 particles, we cloned the remaining particles 10 times (for a total of 120 particles) and restarted the integrations. There are 6 generations in this test run. Our results were scaled from generation to generation so the decay rate can be referenced back to a population of arbitrary starting size. The black dots represent the starting times of various generations. The numbers adjacent to the dots are the generation number. Hence, the second and third generations of this test run start at 60 My and ≈ 270 My, respectively. We terminated the test run at the end of the sixth generation, when the surviving 12 particles had reached 4.34 Gy of cumulative time. The (a, e, i) location of test bodies from this long-lived tail are discussed in Section 5.

The results for all eight of our test runs are shown in Fig. 3. Here we see a second long-lived tail in a different test case after six generations. These two long-lived tails mean there are at least two quasi-stable refugia for particles within the inner Solar System, though it should be pointed out that the particles in both test cases took several hundreds of My or more to find these regions (see Appendix A). The remaining six test

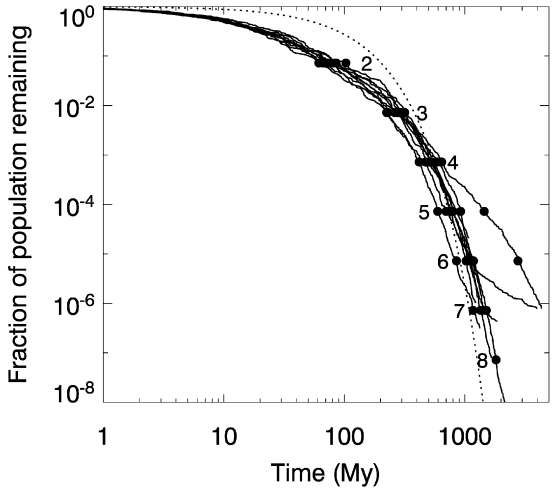

Fig. 3. The dynamical decay rate for 8 different PPP test runs. The initial conditions for each test run is described in Fig. 2. Each test run was tracked for multiple generations until they exceeded 1 Gy of cumulative simulation time. The two test cases that developed long-lived tails were tracked to ~4 Gy. These results indicate there are at least two quasi-stable refugia for particles within the inner Solar System. These zones were not found by our test bodies until the nominal time of the LHB (i.e., 0.6 Gy). The mean of these curves $f_{\rm left}(t)$ at our LHB mileposts (Table 1) at the start of the Nectarian period ($t = 421$ My (4.12 Ga) or 621 My (3.92 Ga)) are 2.1×10^{-3} or 4.0×10^{-4}, respectively, at the beginning of the early-Imbrium period ($t = 631$ My (3.91 Ga) or 691 My (3.85 Ga)) is 3.6×10^{-4} or 2.1×10^{-4}, respectively; and the end of the early-Imbrium period ($t = 721$ My (3.82 Ga) or 821 My (3.72 Ga)) they are 1.7×10^{-4}, and 9.5×10^{-5}, respectively. If we extrapolate the existing trends to $t = 4.6$ Gy, we find that $\sim 2.5 \times 10^{-7}$ of the initial PPP survived 4.6 Gy. The dotted line shows the PPP decay rate for Morbidelli et al. (2001), whose results were proportional to $e^{-t/77}$ with time in My. The curves agree with ours at the critical time of 421–812 My.

cases were terminated at various times after 1 Gy, well beyond the 600–800 My limit for determining the fate of the PPP at the end of the LHB. Despite this, we found no signs that any of these particles found zones where their dynamical lifetimes could grow to anomalously long values. These results provide support for the idea that our runs should do a reasonable job of representing the broad-scale dynamical behavior of PPP populations made of millions of particles.

For reference, we have also plotted the Morbidelli et al. (2001) PPP decay rate of $e^{-t/77}$, with time t in My. We find our results are in good agreement with this estimate for the critical LHB time of $t = 421$–821 My.

Using these eight test cases, we computed the average fraction of the PPP left in the inner Solar System as a function of time. Our results indicate that $f_{\rm left}(t)$ at our LHB mileposts (Table 1) range from 2.1×10^{-3} for the earliest start of the Nectarian period ($t = 421$ My) to 9.5×10^{-5} for the latest termination of the early-Imbrium period ($t = 821$ My). In other words, the size of the PPP drops 3 to 4 orders of magnitude by the time it reaches the basin formation period. As we will show in Section 4.4, inclusion of collisional evolution within the PPP population decreases these values even more.

4.2. The normalized lunar impact rate

The orbital evolution data computed in Section 3 can also be used to compute the impact rate of PPP bodies on the Moon as a function of time. Ignoring collisional evolution within the PPP, we defined the cumulative number of objects striking the Moon between times t_1 and t_2 with a projectile diameter larger than D as:

$$n_{\rm imp}(>D) = \frac{1}{4}\int_D^\infty N_{\rm init}(D)[D_{\rm Moon} + D]^2\,{\rm d}D \times \int_{t_1}^{t_2} P_i(t)\,F_{\rm grav}\big(V_\infty(t), t\big)\,f_{\rm left}(t)\,{\rm d}t. \quad (1)$$

Here $N_{\rm init}(D)$ is the number of PPP objects between D and $D + {\rm d}D$ at $t = 0$ My. Integrating $N_{\rm init}(D)$ over the limits in Eq. (1) yields $N_{\rm init}(>D)$, the cumulative number of initial PPP objects larger than D.

The value $P_i(t)$ is the intrinsic collision probability between test bodies in the PPP and the Moon at time t. This quantity depends solely on the (a, e, i) orbits of both the projectiles and the Moon (Opik, 1951; Wetherill, 1967; Greenberg, 1982; Farinella and Davis, 1992; Bottke and Greenberg, 1993). The gravitational focusing factor for PPP projectiles with the Moon is denoted by $F_{\rm grav}(V_\infty(t), t)$, where $V_\infty(t)$ is the speed of the projectile at time t before the gravitational acceleration by the Earth and Moon is included. The parameter $D_{\rm Moon}$ is the diameter of the Moon.

To calculate the collision probabilities and encounter/impact velocities between bodies in the PPP and the Moon, we applied the methodology described in Bottke et al. (1994b). We assumed the Moon had the same (a, e, i) parameters as the Earth, with the Earth's orbital information given by our numerical integration results. At each output timestep of 10,000 years, we computed the quantities $P_i(t)$ and the velocities $V_\infty(t)$ and $V_{\rm imp}(t)$ between the Moon's (a, e, i) orbit and the (a, e, i) orbits of those test bodies on Earth/Moon-crossing orbits. The mean values of these quantities at each time t were defined as follows: $\langle P_i(t)\rangle_{\rm Cross}$ is the mean P_i value of those test bodies on Earth/Moon-crossing orbits; $\langle V_\infty(t)\rangle$ and $\langle V_{\rm imp}(t)\rangle$ are the mean (weighted by P_i) encounter and impact velocities for the same set of bodies; and $\langle P_i(t)\rangle_{\rm Pop}$ is $\langle P_i(t)\rangle_{\rm Cross} \times \alpha$, where α is the fraction of test bodies at time t on Earth/Moon-crossing orbits. In Eq. (1), we substituted $\langle P_i(t)\rangle_{\rm Pop}$ and $\langle V_\infty(t)\rangle$ for the $P_i(t)$ and $V_\infty(t)$ values.

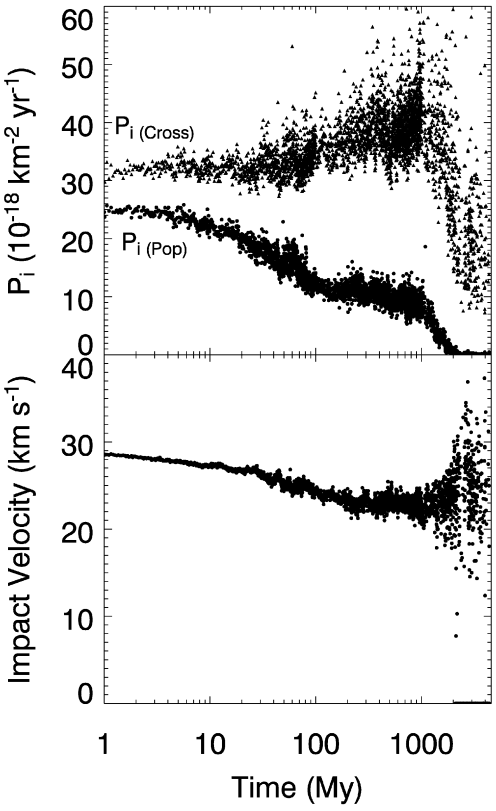

Fig. 4. The mean intrinsic collision probabilities (top) and impact velocities (bottom) between the Moon and test bodies in the PPP. The mean intrinsic collision probability of test bodies on Moon-crossing orbits is labeled as $P_{i\,({\rm Cross})}$, while that of the entire population is $P_{i\,({\rm Pop})}$. The difference between the two values over time shows that the longest-lived test bodies evolve away from Moon-crossing orbits. Note that $P_{i\,({\rm Cross})}$ and the mean impact velocity of test bodies on Moon-crossing orbits only changes by relatively small amounts throughout the simulation.

Fig. 4 shows our results for $\langle P_i(t)\rangle_{\rm Cross}$, $\langle P_i(t)\rangle_{\rm Pop}$, and $\langle V_{\rm imp}(t)\rangle$. We do not show $\langle V_\infty(t)\rangle$ because their values were similar to the $\langle V_{\rm imp}(t)\rangle$ values. We found that $\langle P_i(t)\rangle_{\rm Cross}$ increased from 30×10^{-18} km^{-2} yr^{-1} near $t = 0$ My to 30–46×10^{-18} km^{-2} yr^{-1} near $t = 800$ My. When we factor in α, we find that $\langle P_i(t)\rangle_{\rm Pop}$ decreases from 25×10^{-18} km^{-2} yr^{-1} near $t = 0$ My to $\sim 10 \times 10^{-18}$ km^{-2} yr^{-1} near $t = 800$ My. This indicates that only a small fraction of the PPP is actually capable of impacting the Moon when the early-Imbrium basins were formed. For reference, the lunar impact rate derived from

$\langle P_i(t)\rangle_{\rm Pop}$ near $t = 0-10$ My is similar to that from Morbidelli et al. (2001) (i.e., $\sim 8 \times 10^{-5}$ per My between 0–100 My).

The quantity $\langle V_{\rm imp}(t)\rangle$ decreases from $\sim$29 to $\sim$23 km s^{-1} over $t = 0-821$ My. The reason it drops with time is because the surviving test bodies find zones of stability with higher semimajor axes and lower inclinations than those in the initial PPP. For reference, the mean impact velocities found in Morbidelli et al. (2001) between 0–100 My ranged from 22–25 to $\sim$30 km s^{-1}, depending on the model PPP distribution used in their runs.

We define the gravitational focusing factor between PPP bodies and the Moon in this simulation as:

$$F_{\rm grav}(t) = \left[1 + \frac{v_{\rm esc,M}^2}{v_\infty^2}\right], \quad (2)$$

where $v_{\rm esc,M}$ is the escape speed from the Moon. Note that a completely rigorous definition would also include a correction factor that accounts for gravitational focusing produced by Earth's gravity at the Moon's distance as well as how the Moon's distance r changes between the Moon-forming impact and the end of the simulation (e.g., Touma and Wisdom, 1994; Ward and Canup, 2000). These factors are negligible for the PPP, however, because $\langle v_\infty\rangle$ is well over 20 km s^{-1} (i.e., comparable to $\langle V_{\rm imp}(t)\rangle$). Accordingly, the gravitational focusing factor $F_{\rm grav}(t) \approx 1$.

Fig. 5 shows the number of lunar impacts between 0 and 1,200 My as a function of time for a PPP population normalized to be comprised of a single body. Because we assume PPP dynamics is independent of its mass, this function can be multiplied by any PPP population of choice to obtain the number of lunar impacts occurring at a given time after the Moon's formation. These results assume that the projectiles striking the Moon are substantially smaller than the Moon itself (i.e., $D_{\rm moon} \gg D$). We find that the PPP impact rate drops by two orders of magnitude over the first 100 My. It then enters into a slower decline between 100 and 1200 My. A line in log-linear space fit to the results between $t = 100$ and 1200 My has the form $\log_{10}[n_{\rm imp}(>D)/N_{\rm init}(>D)] = -5.6 - 0.0038t$, with t in units of My.

It is instructive to compare the values in Fig. 5 to those in Fig. 8.6.1 of Hartmann et al. (1981), who plotted the density of $D > 4$ km craters per square km on the Moon vs their estimated crater retention age (see also Neukum and Ivanov, 1994; Stöffler and Ryder, 2001). We find that our numerically derived lunar impact rate decreases by over 4 orders of magnitude between $t = 0$ and 721–821 My, while the crater density-age relationship of Hartmann et al. (1981) only drops by $\sim$2 orders of magnitude over roughly the same time interval. If the Hartmann et al. (1981) estimates were not influenced by crater saturation, our PPP impact flux drops off too quickly to reproduce their results.

Using Fig. 5, we can derive the number of PPP impacts on the Moon needed to produce basin sets A and B over the time intervals described in Table 1 as a function of $N_{\rm init}(>D)$. For reference, the total number of basin-forming impacts from $t_1 = 0$ My to $t_2 = 1200$ My is $\log[n_{\rm imp}(>D)/N_{\rm init}(>D)] \approx -2.837$. For basin set A, $\log[n_{\rm imp}(>D)/N_{\rm init}(>D)]$ ranges from -5.218 to -6.156, while for basin set B, it goes from -6.066 to -6.853. These values are used in the next section.

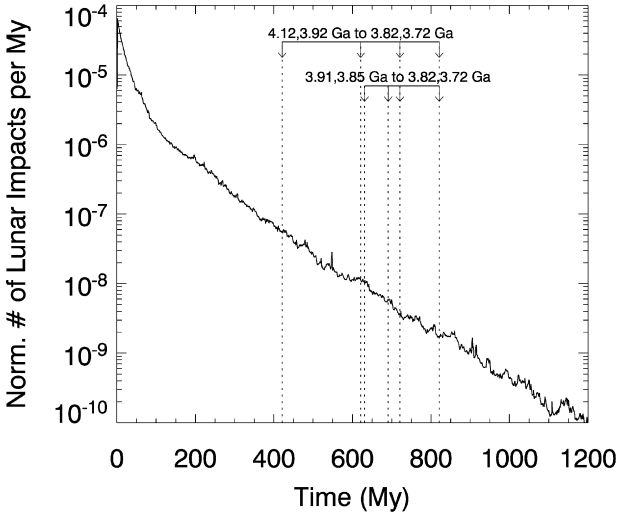

Fig. 5. The number of lunar impacts produced per My by the PPP, where the size of the PPP has been normalized to a single object. The $t = 0$ My time was assumed to be the Moon-forming event. The PPP impact rate drops sharply over the first 100 My and then transitions to a more steady decline between 100 to 1200 My. The largest lunar basins formed in Nectarian and early-Imbrium time periods are, in order of decreasing size, Imbrium, Orientale, Serenitatis, and Nectaris. The plausible formation intervals for basin sets A and B are given in Table 1. The interval with a maximum at 4.12 Ga and a minimum at 3.72 Ga corresponds to basin set A. The interval with maximum at 3.91 Ga and minimum at 3.72 Ga corresponds to basin set B. No basins formed after these times.

4.3. The probability of basin formation by a collisionless post-planet formation population

4.3.1. Estimating the initial size of the post-planet formation population

In Section 4.2, we computed the number of basin-forming impacts over a given time interval as the ratio $\log[n_{\rm imp}(>D)/N_{\rm init}(>D)]$. We can now use constraints from basin sets A and B to determine $n_{\rm imp}(>D)$. In turn, this allows us to estimate the optimum size of an initial, collisionless PPP population $N_{\rm init}(>D)$ capable of making those basins.

The energy needed to produce the Imbrium basin was $1-3 \times 10^{33}$ ergs, while the energy needed to make Orientale, Serenitatis, and Nectaris was $\sim 1 \times 10^{33}$ ergs (see Section 2.3). If we assume these basins were formed by the PPP, we can use Fig. 4 to estimate the impact velocities of the basin-forming projectiles. Fig. 4 shows that $\langle V_{\rm imp}(t)\rangle$ between $t = 421-812$ My was $\sim$23 km s^{-1}. This implies that the PPP projectile capable of forming Imbrium had a mass of $(8 \pm 4) \times 10^{20}$ g, while those capable of forming Orientale, Serenitatis, and Nectaris were $\sim 4 \times 10^{20}$ g. If the PPP projectiles had a bulk density comparable to S-type asteroids (2.7 g cm^{-3}; Britt et al., 2002), these values yield projectile diameters of $D = 64-93$ km for Imbrium and $D \sim 64$ km for the other large basins. Accordingly, to explain these basins as a byproduct of PPP impacts, we need four $D > 64$ km projectiles to strike the Moon during the Nectarian and early-Imbrium periods to make basin set A ($n_{\rm imp}(D > 64\,{\rm km}) \approx 4$), while two $D > 64$ km projectiles must

strike the Moon during the early-Imbrium period to make basin set B.

We now have everything we need to solve for $N_{\rm init}(D > 64$ km). Using the time intervals for basin set A described in Table 1, we estimate that $N_{\rm init}(D > 64\,{\rm km})$ could range from 0.66 to 5.8×10^6. For basin set B, these values range from 2.3 to 14×10^6.

To estimate the total mass represented by these putative PPPs, we need to estimate the shape of their size-frequency distributions. We will assume that (i) the largest bodies in the PPP were probably not much bigger than the Asteroid Ceres ($D = 930$ km) and (ii) the shape of the size-frequency distribution for the PPP was similar to that found now in the main belt. We consider assumption (i) reasonable because planet formation and asteroid belt evolution models indicate that most Moon- to Mars-sized planetary embryos were accreted or scattered by the planets prior to the Moon-forming impact (e.g., Petit et al., 2001). For assumption (ii), Bottke et al. (2005a, 2005b; 2006a) found that small body populations undergoing a nominal degree of collisional evolution take on a wave-like shape reminiscent of the main belt size distribution (see Section 5 as well as Strom et al., 2005). While we cannot say for certain that the PPP had the exact same shape as the main belt size distribution, it seems plausible that the conditions that produced the main belt size distribution were not very different from those that formed the planetesimal size distribution in a nearby region of the Solar System.

The main belt population described in Bottke et al. (2005a) contains roughly 510 bodies with $D > 64$ km. From the $N_{\rm init}(D > 64$ km) estimates described above and the time intervals in Table 1, we conclude that an initial PPP producing basin set A was 1300–11,000 times larger than the current main belt. Assuming the main belt has a mass of $\sim 5 \times 10^{-4}\ M_\oplus$, this means the initial PPP population had to contain 0.6–6 Earth masses. Because the constraints of basin set B are more restrictive, the PPP making those basins requires 4600–28,000 times the current main belt population, or from 2 to 14 Earth masses of material.

The best estimate of the initial mass of the Solar Nebula in the inner Solar System is a few Earth masses at best (e.g., Weidenschilling, 1977). Thus, if basin sets A and B formed over the narrowest time intervals described in Table 1, the starting PPPs require too much mass to be considered reasonable sources of the LHB, even without including collisional evolution in the PPP.

4.3.2. *Monte Carlo simulations of lunar basin formation by collisionless post-planet formation populations*

The next task is to move away from the idealized calculations above and instead model lunar basin formation using the LHB constraints described at the end of Section 2.3. This can be accomplished using Monte Carlo simulations. We assume that individual basin-forming events capable of making $D_{\rm crater} > 900$ km occur at random times according to the impact rate distribution in Fig. 5. The starting PPP impact rate distribution for each test case was determined by multiplying the normalized collisionless impact rate in Fig. 5 by an arbitrary mass factor (Fig. 6a). Starting PPP masses were assumed to be between 0.005 and $50 M_\oplus$, with the higher values added for completeness' sake; we recognize that self-gravity and collisional damping among large and essentially unrealistic PPPs would force them to evolve in a very different manner than those of smaller PPPs.

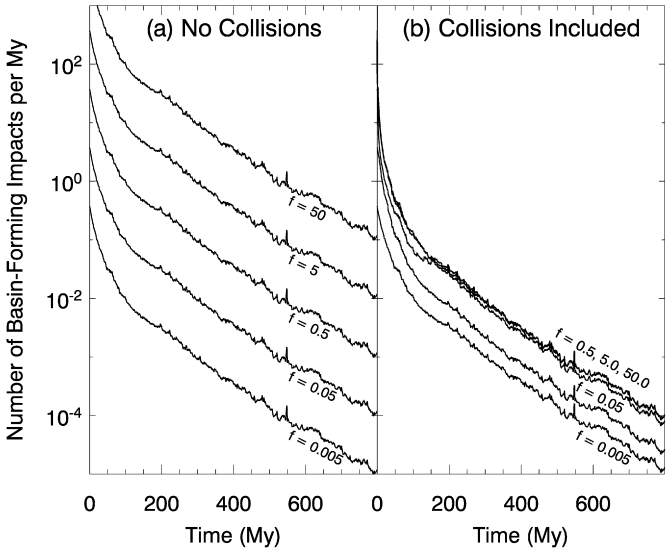

Fig. 6. The formation rate of lunar basins with $D_{\rm crater} > 900$ km produced by various post planet-formation populations (PPPs). The starting mass for each PPP was $f = 0.005$–$50 M_\oplus$. (a) The basin rate formation distribution for collisionless PPPs. These values were determined by scaling the normalized lunar impact rate distribution from Fig. 5 by an appropriate factor. (b) The basin rate formation distribution for PPPs between 0.005–$50 M_\oplus$ that experienced collisional evolution. To account for the stochastic nature of breakup events in the PPP over time, we ran each size distribution through our collisional and dynamical depletion evolution model CoDDEM 20 times with different random seeds. The results were then averaged and the impact rate computed (see Section 4.4). Collisional grinding significantly depletes PPPs with large starting masses ($f = 0.05$–$50 M_\oplus$) over the first few tens of My. The consequence is that few are capable of producing the Nectarian and early-Imbrium basins.

The timing of basin formation on the Moon in the Monte Carlo code is controlled by random deviates. A successful run is one in which the correct number of Nectarian and/or early-Imbrium basins (basin sets A and B) are formed in the appropriate time intervals and no Orientale-sized basin is formed after the end of the early-Imbrium period (constraints #2–#3; Section 2.3). The probability of success for each starting PPP was determined by running our Monte Carlo simulation 3000–100,000 times using different random seeds.

Figs. 7a and 8a show results for basin sets A and B, respectively, vs the various formation time intervals described in Table 1 and Section 2.3. The peaks of the probability distribution for the longest time intervals reach 10–20% and correspond to the optimum PPP masses estimated using the methods described in Section 4.3.1. The odds of success quickly decrease as we move away from these peaks. For example, massive PPPs have low probabilities because they tend to make younger basins than those observed (i.e., in violation of constraint #3; Section 2.3). For the shortest time intervals, the peaks of the probability distribution for both basin sets A and B are limited to values between 1–10%.

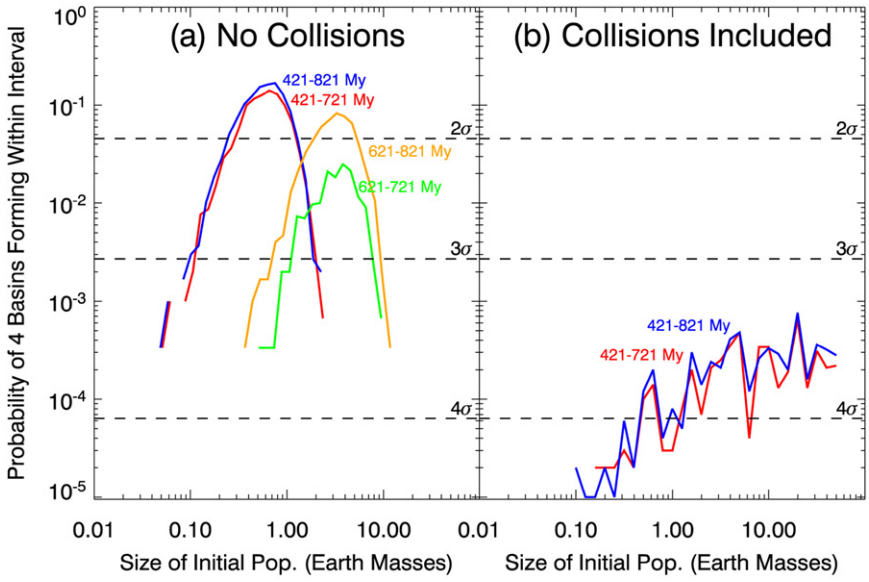

Fig. 7. The probability that post planet-formation populations (PPPs) of varying starting masses will produce the four large basins found in the Nectarian and early-Imbrium periods (i.e., basin set A from Section 2.3: Imbrium, Nectaris, Orientale, and Serenitatis). The basins were assumed to have formed from 4.12 or 3.92 Ga to 3.82 or 3.72 Ga ($t = 421$ or 621 My to 721 or 821 My) (Table 1). The values were computed using a Monte Carlo code run 3000–100,000 times (see Sections 4.3.2 and 4.4.2 for details). A successful test case was defined as one in which all four basins were formed in the labeled time interval and no basins were formed after the end of the interval. (a) The success probabilities for PPP runs without collisional evolution. (b) The success probabilities for PPP runs in which collisional evolution is included. Note that collisional evolution reduces the likelihood of a successful outcome in the declining bombardment paradigm below the 3σ threshold. No successful runs were found for 621–721 My and 621–821 My intervals.

Overall, these results indicate that a collisionless PPP has a small but non-negligible chance to create the Nectarian and early-Imbrium basins, but only if the initial population had 0.4 to several $M_{\oplus}$ of material in the form of $D < 1000$ km bodies. Even then, much depends on the timing of the basin formation events in basin sets A and B. Advocates of the terminal cataclysm scenario could argue that the PPP masses with the highest probabilities are unlikely to exist in the inner Solar System after the Moon-forming event. As we will see in the next section, however, it is unnecessary to employ such arguments because collision evolution among PPP bodies has a important negative effect on the results.

Before moving on, it is useful to check these results against reality. For our first check, we computed the total number of Orientale-sized basins made on the Moon. Using our Monte Carlo simulations with the highest probability of success and basin set A constraints, we predict that the declining bombardment paradigm should have produced 100–700 $D_{\rm crater} >$ 900 km basins in the pre-Nectarian period, defined here as the interval between the formation of the lunar crust 4.46 ± 0.04 Ga (Norman et al., 2003) and the formation of Nectaris (see Section 2.3). Using basin B constraints alone, the number of $D_{\rm crater} > 900$ km basins created in the pre-Nectarian and Nectarian periods is 340–600. These numbers are exceedingly high compared to observations (Wilhelms, 1987; Baldwin, 2006). This discrepancy, however, might be eliminated if the largest pre-Nectarian basins were in saturation equilibrium, with newly-created basins covering up and/or erasing older basins. At present, we cannot say whether this scenario is consistent with existing lunar data.

For our second check, we examined the South-Pole Aitken basin constraint described at the end of Section 2.3 (point #4). Using the procedure described in Section 4.2, we find that South Pole-Aitken-like formation energies of $0.25-4 \times 10^{34}$ ergs (Section 2.3) require the impact of PPP projectiles with $90 < D < 220$ km. If the shape of the PPP size distribution was indeed comparable to that in the observed main belt, the declining bombardment should have produced tens of South Pole-Aitken-like basins. Given the extreme depth and unique nature of South Pole-Aitken itself, it seems unlikely that these putative basins could have completely escaped detection on existing lunar topographic maps (Smith et al., 1997; Cook et al., 2000).

4.4. Collisional evolution within the post-planet formation population

Numerical modeling work has shown that dynamically excited small body populations in the inner Solar System significantly larger than the main belt population are highly efficient at losing mass via catastrophic disruption events (e.g., Bottke et al., 2005a, 2005b, 2006a). These factors imply that the PPPs modeled in Section 4.3 should undergo a rather intense phase of collisional evolution, perhaps enough to dramatically modify the number of $D > 64$ km objects available to create lunar basins. Here we explore what happens to our declining bombardment model results if we include collisions between bodies in the PPP.

Before starting, it is useful to point out a few caveats relevant to our more extreme test cases. For simplicity, we have assumed in this paper that (i) collisions do not affect the dy-

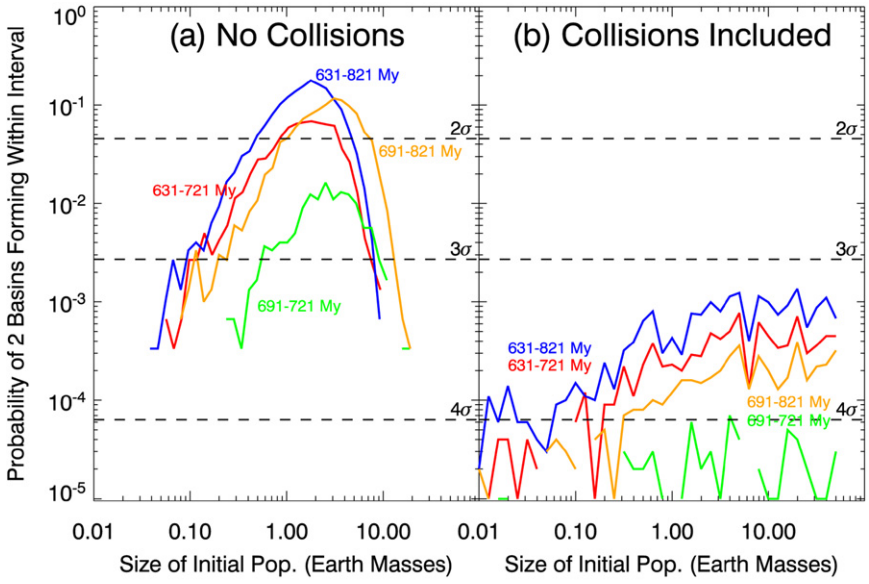

Fig. 8. The probability that post planet-formation populations (PPPs) of varying starting masses will produce the basins Imbrium and Orientale in the early-Imbrium period (i.e., basin set B from Section 2.3). The basins were assumed to have formed from 3.91 or 3.85 to 3.82 Ga or 3.72 Ga ($t = 631$ or 691 My to 721 or 821 My) (Table 1). See Fig. 7 for additional details. (a) The success probabilities for PPP runs without collisional evolution. (b) The success probabilities for PPP runs in where collisional evolution is included. As in Fig. 7, collisions are effective at reducing the success probabilities for the declining bombardment paradigm below the 3σ threshold.

namics of the PPP and (ii) PPP dynamics is accurately modeled using massless test bodies. These assumptions break down for extremely massive PPPs. In such systems, mutual collisions can damp the orbital excitation of the PPP, while collective gravitational effects modify the orbital evolution of the PPP in ways that are not simulated here. Hence, while we model the evolution of very massive PPPs using our codes, the outcomes from these particular runs should not be considered accurate; they are merely included for completeness' sake. (Note that super-massive PPPs can be ruled out according to Solar Nebula constraints; Weidenschilling, 1977.)

4.4.1. A demonstration of the effects of collisional evolution on the PPP

To demonstrate how collisions can affect the PPP over time, we describe a representative test case. We will assume that basin set A formed between 4.12–3.72 Ga ($t = 421-821$ My) and was produced by an initial PPP that contained $\sim 0.6 M_\oplus$ in the form of $D < 1000$ km planetesimals. This starting mass produced the optimum probabilities found in Fig. 7a. For reference, this value is $\sim 6-8$ times larger than the estimated population of $D < 1000$ km bodies in the primordial (not the current) main belt population (Bottke et al., 2005a, 2005b).

Catastrophic disruption events within the PPP were tracked using the 1-D collisional evolution code CoDDEM (Collisional and Dynamical Depletion Evolution Model) described in Bottke et al. (2005b). This code accepts as input an initial size-frequency distribution where the population has been binned between 0.001 km $< D <$ 1000 km in logarithmic intervals $d \log D = 0.1$. The particles in the bins are assumed to be spherical and are set to a bulk density of 2.7 g cm^{-3}. CoDDEM computes how collisions, fragmentation, and dynamical effects modify this size distribution over a selected time interval. For additional details about CoDDEM, see Bottke et al. (2005a, 2005b). Note that the accuracy of CoDDEM's results has been checked by modeling the evolution of the main belt population and matching numerous constraints.

Two parameters used as input for CoDDEM include the intrinsic collision probabilities (P_i) and impact velocities ($V_{\rm imp}$) of PPP bodies colliding with one another. We obtained these values using the test runs described in Sections 3–4. At each timestep, we computed P_i and $V_{\rm imp}$ between all possible pairs of test bodies on crossing orbits (Bottke et al., 1994a). These bodies tend to have high velocities with respect to one another, a byproduct of their high inclinations. Overall, we found that reasonable representative values for our runs over time were $P_i \sim 15 \times 10^{-18}$ km^{-2} yr^{-1} and $V_{\rm imp} \sim 20$ km s^{-1}.

We assumed our initial PPP size-frequency distribution followed the same trends as those determined for the primordial main belt from dynamical and collisional models (Bottke et al., 2005a, 2005b). The initial size distribution of the PPP for $D \sim 100-1000$ km planetesimals was set to $\sim$1200 times the current main belt population ($0.6 M_\oplus$) and was given a differential power law index $q \sim -4.5$, the same as the observed main belt over the same size range (see Bottke et al., 2005a, 2005b). For $D < 100$ km, we assumed a shallow initial slope ($q = -1.2$). The shape of this population can be found in Fig. 9 at $t = 0$ My. It is important to point out that the shape of this size distribution is a favorable one for *minimizing* collisional evolution. If we had extended the $q = -4.5$ slope to diameters smaller than $D < 100$ km, the degree of comminution in the PPP would have been even more severe.

Our runs neglect collisional evolution among PPP planetesimals prior to the Moon-forming impact (at $t = 0$ My). We believe this approximation has minimal impact on our results

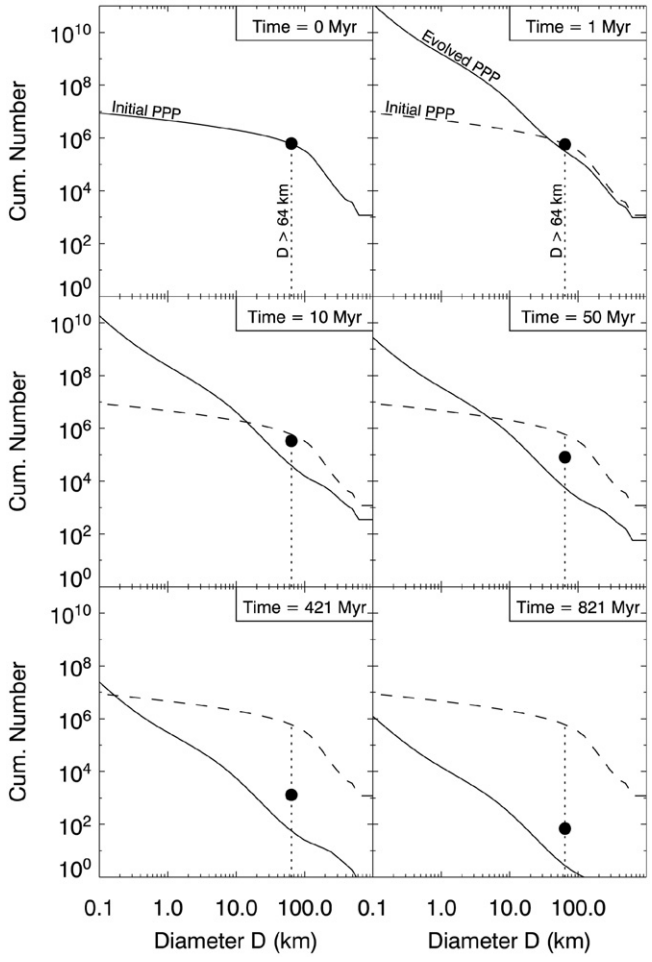

Fig. 9. The collisional evolution and dynamical depletion of the post-planet formation population (PPP) in which the initial mass is $0.6M_{\oplus}$ (see Section 4.3). The $t = 0$ My timestep shows the initial shape of the PPP size distribution, which was generated using results from Bottke et al. (2005a, 2005b). The dashed vertical line corresponds to $D > 64$ km projectiles, the size needed to make the four largest Nectarian and early-Imbrium basins. The black dot shows what the depletion of $D > 64$ km projectiles would be when collisional evolution is excluded. The bump observed in most frames near $D \sim 2$-4 km is driven by asteroid disruption scaling law, which undergoes a transition at $D \sim 0.2$ km between the strength and gravity-scaling regimes. The intermediate timesteps show how quickly comminution can reduce the initial population in addition to the bodies lost from dynamical depletion. By the $t = 421$ and 821 My timesteps, collisional evolution has reduced the number of $D > 64$ km objects in the PPP by nearly a factor of 20 below the expected depletion produced by dynamics alone. Accordingly, only a few $D > 64$ km projectiles are left in the PPP to produce the large Nectarian and early-Imbrium basins in this interval.

because we are mainly concerned with the size of the PPP between $t = 421-821$ My. Tests indicate that adding an extra ~30 My of comminution to the beginning of our CoDDEM runs does not significantly affect the PPP after $t >$ 421 My.

The dynamical loss of PPP planetesimals from the inner Solar System was also included in CoDDEM. At every timestep, which was 50,000 years or less depending on the rate of collision events taking place within the code, we removed the appropriate fraction of the PPP across all size bins based on the numerically-derived decay rates described in Section 4.1 (see Fig. 3). To compare collision/no-collision test cases, the depletion level of a $D > 64$ km population experiencing zero collisions is plotted as a black dot in Fig. 9.

Fig. 9 shows several snapshots of the collisional evolution of the PPP between $t = 0$ and 821 My. After 1 My, collisions among large asteroids have created numerous smaller fragments that increase the slope of the $D < 100$ km size distribution. Catastrophic disruption events among the PPP also generate a bump in the size distribution near $D \sim 3-4$ km. The bump is a by-product of the "V"-shaped asteroid disruption function that shifts from strength- to gravity-scaling regimes near $D = 0.2$ km (e.g., Durda, 1993; Campo Bagatin et al., 1994; Durda et al., 1998; Davis et al., 2002; O'Brien and Greenberg, 2003; Bottke et al., 2005a, 2005b). At smaller sizes, the PPP enters into a Dohnanyi-like collisional equilibrium (Dohnanyi, 1969) with a differential power law index near −3.6 (e.g., O'Brien and Greenberg, 2003).

At $t = 10$ and 50 My, we find that collisional and dynamical evolution have significantly depleted the $D > 64$ km population, with the original PPP dropping to 0.07 and 0.01 of the initial PPP, respectively. Only a portion of this is from dynamical loss mechanisms; we find that the fraction of the PPP dynamically removed from the inner Solar System at these times is 0.51 and 0.13. This means that collisional grinding is responsible for most of the $D > 64$ km bodies removed from the PPP at these times.

By $t = 421$ and 821 My, collisional and dynamical processes have reduced the number of $D > 64$ km bodies in the PPP to 9.8×10^{-4} and 4.7×10^{-6} of the initial PPP, respectively. For reference, the fraction of the PPP left by dynamics alone should be 1.9×10^{-3} and 9.5×10^{-5}, respectively. This means that 95% of the $D > 64$ km bodies were eliminated from the PPP via collisional evolution. Even without running our Monte Carlo code, it is clear that this drop in the available number of basin-forming projectiles should produce much lower success probabilities than those found in Fig. 7a.

One could try to compensate for this difference by increasing the initial PPP by an additional factor of 20 at the start of the runs. Such an increase, however, would be unlikely to help us match constraints. First of all, it would make the initial size of the PPP equivalent to ~11 Earth masses, far in excess of Solar Nebula constraints for the terrestrial planet region (Weidenschilling, 1977). Second, a massive population like this one would most likely experience (i) an intense collisional phase, enough that the orbital excitation of the population would be damped and (ii) strong mutual gravitational interactions between PPP bodies. We are unsure what would happen in this hypothetical situation, but it is clear that the resulting system would not resemble our terrestrial planet system.

These results lead us to predict that this particular PPP is unlikely to have produced the Nectarian and early-Imbrium basins (basin sets A or B) during any of the time intervals described in Table 1.

4.4.2. Monte Carlo simulations of lunar basin formation using collisionally evolved post-planet formation populations

Returning to the Monte Carlo code described in Section 4.3.2, we now examine how collisions within the PPP affect the role of lunar basin formation. Input for this code was obtained by using CoDDEM to track the collisional evolution and dynamical depletion of PPP size distributions with initial masses $0.01-50M_{\oplus}$ from $t = 0$ to 1200 My. We determined the initial size distributions for these PPPs by multiplying the size distribution shown in the $t = 0$ My timestep from Fig. 9 by an appropriate "mass" factor. Because catastrophic disruption events are stochastic, these PPP size distributions were run through CoDDEM 20 times with different random seeds for each run. The number of $D > 64$ km bodies tabulated at every output timestep was then averaged across the runs and multiplied by the normalized lunar impact rate distribution described in Section 4.1 (Fig. 5). A representative sample of the PPP basin formation rate distributions obtained from this method is shown in Fig. 6b.

These results indicate that collisional evolution within the PPP has a dramatic effect on lunar basin formation. In Fig. 6b, we see that test runs with starting masses between 0.05 and $50M_{\oplus}$ undergo an intense phase of collisional evolution and rapid depletion within the first few My of their existence. These populations effectively self-destruct, leaving behind few $D >$ 64 km planetesimals capable of creating the observed Nectarian and/or early-Imbrium basins. Moreover, we find that large starting masses for the PPP produce an increased number of catastrophic disruption events, such that the $0.5-50M_{\oplus}$ runs produce comparable numbers of basins for the intervals listed in Table 1.

When these data are input into our Monte Carlo code, we find the probability of reproducing the Nectarian and/or early-Imbrium basins drops precipitously from that found in Section 4.3.1. Figs. 7b and 8b show results for basin sets A and B, respectively. The highest probability for success over the tested basin formation time intervals is only ≈0.1%, much smaller than the results from the no-collision scenario (Figs. 7a and 8a).

Overall, we found that collisional evolution prevents PPPs with large starting masses from providing significant numbers of basin-forming projectiles to the Moon during the Nectarian and early-Imbrium periods. This explains why our Monte Carlo simulations cannot match constraints at the 3σ confidence level in basin sets A or B, regardless of our choice of starting PPP mass. More positively, these runs only produce on the order of 10 Orientale-sized basins and a few South Pole-Aitken-like basins in the pre-Nectarian period. These runs provide a better match to our reality check (constraint #4) than those from Section 4.3.1.

In summary, the declining bombardment as modeled here cannot match the constraints from either basin set A or B. We believe these are sufficient grounds to reject it as a plausible model for the LHB. This leaves the terminal cataclysm as the best available paradigm for producing the late-forming lunar basins. The only terminal cataclysm model capable of matching LHB constraints at present (as well as other Solar System constraints) is the Nice model described in Section 2.1.

5. Conclusions and implications

In this paper, we used several different numerical simulations to examine whether the declining bombardment paradigm for producing the LHB was consistent with constraints provided by the largest lunar basins formed during the Nectarian and early-Imbrium periods (Nectaris, Serenitatis, Imbrium, and Orientale; basin set A) and during the early-Imbrium period alone (Imbrium and Orientale; basin set B) (see Section 2.3 and Table 1). Basin set B was explicitly used to ensure that any controversies about the ages of Nectaris and Serenitatis did not affect our results. Our methods allowed us to reexamine the numerical modeling work and LHB constraints described in Morbidelli et al. (2001). We assumed the energy needed to produce the Imbrium basin was assumed to be $1-3 \times 10^{33}$ ergs, while the energy needed to make Orientale, Serenitatis, and Nectaris was $\sim 1 \times 10^{33}$ ergs (see Zahnle and Sleep, 1997).

Our model of the declining bombardment population (i.e., PPP) was assumed to be comparable to high inclination asteroids from the observed NEO population with $a < 2$ AU and $i > 40°$. It was tracked using numerical integration codes until most of its test bodies had been dynamically eliminated. The remnants were then cloned and restarted. We followed multiple generations of this population for at least 1 Gy and, in some cases, >4 Gy. At the same time, we computed their collision probabilities and impact velocities with the Moon between $t = 0$ My (defined here as the Moon-forming event) and the end of our simulations (Fig. 3). This yielded the information needed to compute the normalized lunar impact rate distribution for the PPP (Fig. 5). The number of Orientale-sized and larger basin-forming impacts on the Moon was found to drop off precipitously over the first 100 My of the simulation before transitioning into a more steady decline between 100–1200 My. Using the lunar impact velocity results and the basin formation energies described above, we estimated that $D > 64$ km projectiles would be needed to produce Imbrium, Orientale, Serenitatis, and Nectaris.

Using codes described in Bottke et al. (2005a, 2005b), we tracked how PPPs of varying starting mass were affected by collisional evolution and dynamical depletion between $t = 0$ and 1200 My. Mutual gravitational effects and collisional damping of orbital e, i's within the PPP were ignored, though these mechanisms are only likely to affect massive PPPs that are already inconsistent with Solar Nebula constraints. Our results, when combined with our normalized lunar impact rate distribution, were input into a Monte Carlo code in order to track the likelihood that basin sets A and B were created over various time intervals. As an added constraint, we rejected solutions in which basins were formed after the end of the early-Imbrium period.

Our results indicate that the declining bombardment paradigm as modeled here is extremely unlikely to have formed the Nectarian and early-Imbrium basins and can be ruled out at the 99.7% (3σ) confidence level for all of the basin formation time intervals described above (Figs. 6a and 6b). Our solutions are independent of the starting mass of the PPP. These results lead us to conclude that the declining bombardment did not pro-

duce the Moon's late-forming basins and thus cannot explain the LHB. In contrast, the Nice terminal cataclysm model for the LHB described in Section 2.1 appears to be viable from a dynamical modeling perspective and is consistent with existing constraints.

These results have several important implications for our understanding of the chronology of events that occurred early in Solar System history. If the LHB did not come from the declining bombardment, it implies that the lunar (and terrestrial) impact rate in the interim between the Moon-forming impact and the LHB was lower than previously thought, at least in terms of basin-forming events. This may allow us to glean new insights into the measured shock degassing ages of lunar samples between 4.5–3.9 Ga (e.g., Bogard, 1995; Grinspoon, 1989; Hartmann, 2003; Chapman et al., 2007).

If any pre-Nectarian basins were produced by the PPP, they most likely formed relatively soon after the Moon-forming impact. This would provide the easiest explanation for the curious absence of secondary overgrowths on Hadean-era terrestrial zircons prior to ∼4.0 Ga (Trail et al., 2007; see Section 2.1). A paucity of lunar and terrestrial impactors between 3.9–4.4 Ga would also imply that pre-Nectarian basins like South Pole-Aitken either had to form earlier than the oldest terrestrial zircons ($\geqslant$4.4 Ga) or during the LHB epoch ∼3.9 Ga. While insufficient information exists to further constrain the ages of the pre-Nectarian basins, we argue that the paucity of lunar impact melt clasts and crustal rocks older than 3.8–4.0 Ga is most consistent with a large number of pre-Nectarian basins forming during the LHB (Ryder et al., 2000; Stöffler and Ryder, 2001; Cohen et al., 2000; Cohen, 2002; see also Kring and Cohen, 2002). It also provides the easiest way to explain why multiple basin-forming events occurred on the Moon 3.75–3.95 Ga (Norman et al., 2006).

If the declining bombardment paradigm is indeed inoperable, it may have important implications for the estimated formation times of basins on Mercury and Mars. For example, a commonly used chronology for features on Mars assumes a steadily declining bombardment between 4.5–3.8 Ga was the source of the oldest basins and craters (e.g., Neukum and Ivanov, 1994; Hartmann and Neukum, 2001; Neukum et al., 2001a). If Mars had an impact history analogous to that of the Moon, however, many of the oldest and largest martian craters may have formed in a terminal cataclysm occurring during an abbreviated period ∼3.9 Ga. It is likely that many of the buried basins discovered in the Mars Observer Laser Altimeter (MOLA) data formed during this epoch as well (Frey et al., 2002; Buczkowski et al., 2005; Frey, 2006). The estimated age of basins and features on Mercury would be similarly affected (Strom and Neukum, 1988; Neukum et al., 2001b). This scenario also raises the possibility that most of the morphology existing on Mars or Mercury prior to ∼3.9 Ga was obliterated by the LHB and thus is permanently hidden from our view. If true, it is plausible that most of the early events still observable on the martian surface took place over a more compressed timescale than previously thought. We believe a revised martian chronology based on the Nice terminal cataclysm model (Section 2.1) might help us glean many new insights into ancient martian history.[1]

Acknowledgments

We thank Don Bogard, Clark Chapman and Steve Mojzsis for their helpful discussions and insights into many of the issues related to the Late Heavy Bombardment. We also thank Alessandro Morbidelli and Kleomenis Tsiganis for their careful, constructive, and useful reviews. Research funds for William Bottke were provided by NASA's Origins of Solar Systems Program (Grant NAG5-10658) and NASA's Planetary Geology and Geophysics Program (Grant NAG513038).

Appendix A. Long lived niches for inner Solar System asteroids

The current configuration of planets in the inner Solar System contains several regions of phase space where small bodies can survive for timescales considerably longer than the typical lifetimes of NEOs (e.g., see Hartmann et al., 2000, for a review). The most well-known ones are stable and contain asteroids today: the main asteroid belt, the high inclination Hungaria and Phocaea asteroids at ∼1.7−1.9 AU and 2.3–2.5 AU, respectively; the Hilda and Thule asteroids in the 3:2 and 4:3 mean motion resonances with Jupiter, respectively; and the Mars- and Jupiter-Trojan asteroids. Others have only recently been discovered using numerical integration methods and may or may not be stable over timescales approaching the age of the Solar System. For example, Evans and Tabachnik (1999, 2002) tracked the orbits of test bodies on nearly-circular, low-inclination orbits throughout the inner Solar System and found that some objects placed between 0.09–0.21 and 1.08–1.28 AU can survive at least 100 My (see also Hartmann et al., 2000). The former region is the putative home of the vulcanoid asteroids (e.g., Leake et al., 1987; Stern and Durda, 2000; Vokrouhlický et al., 2000). At present, we have yet to positively identify an *indigenous* body in either region. A few candidate objects have been spotted in the 1.08–1.28 AU region (Evans and Tabachnik, 1999, 2002), but these objects may also be temporarily trapped in minor resonances that intersect the region (e.g., Bottke et al., 2002). Extensive searches for Vulcanoid asteroids are on-going (e.g., Durda et al., 2000).

Our results from Fig. 3 indicate there are at least two additional long-lived niches reachable by small bodies in the inner Solar System. They have been in place as long as the planets

[1] As follow-up to this idea, it is interesting to consider whether a terminal cataclysm brought large quantities of volatiles to Mars ∼3.9 Ga. Levison et al. (2001) predicted that comets striking Mars during the LHB delivered $\sim 6 \times 10^{22}$ g of material. Because much of this material would consist of various ices, these impacts would have transported considerable water to Mars and would have produced a temporary CO_2 atmosphere with surface pressures greater than 1 bar (Stern and Levison, 1999). Individual impacts would have also distributed warm ejecta around the planet, enough to heat surface ice and even inject steam into the atmosphere (Segura et al., 2002). Collectively, these effects might have induced prolonged periods where rainfall was possible. Hence, Mars' inferred early wet environment may have been a direct byproduct of the LHB.

have had their current configuration. They were identified in our runs by their shallow decay curves that break away from the other test runs at ∼0.6 and 1.2 Gy. The 0.6 Gy tail, which is also seen in Fig. 2, is characterized by test bodies with orbital parameters $a = 2.13-2.16$ AU, $e = 0.16-0.30$, and $i = 17°-26°$. Note that this region lies directly between the stable Hungaria and Phocaea asteroid regions. Fig. 10 shows the orbital evolution of a single test body that wandered into this region. The test body in question was a third generation clone that stayed at high inclinations with $a < 2$ AU for several hundreds of My. Eventually, a planetary close encounter (most likely with Mars) moved it to an $a > 2$ AU orbit, where further Mars encounters and dynamical resonances drove the body to the a, e, i parameters described above. In contrast, the 1.2 Gy tail is characterized by test bodies with orbital parameters $a \approx 2.29$ AU, $e = 0.15-0.30$, and $i = 23°-30°$. This sub-population was produced by a sixth generation test body that found a tiny resonance intersecting the Phocaea asteroid region. A portion of its orbital traverse is shown in Fig. 11.

In hindsight, it is perhaps no surprise that the most long-lived test bodies in our simulations are those that reached orbits near the stable Hungaria and Phocaea asteroid regions. These long-lived niches are far from Venus, Earth, or Jupiter-crossing orbits. As seen in Fig. 4, however, the trade-off is that these PPP survivors are unlikely to re-emerge from this region to strike the Moon.

A search for asteroids in our two refugia yields the following information. There are 10 bodies with absolute magnitude $15 < H < 19$ that have orbital parameters consistent with the 0.6 Gy long-lived tail ($a = 2.13-2.16$ AU, $e = 0.16$–0.30, and $i = 17°-26°$) and 15 bodies with $14 < H < 16$ that have orbital parameters consistent with the 1.2 Gy long-lived tail ($a \approx 2.29$ AU, $e = 0.15-0.30$, and $i = 23°-30°$). The spectroscopic signature of these bodies may eventually help us identify where they came from and the dynamical mechanisms that put them there.

At present, we cannot say whether these two long-lived niches and the regions that surround them, let alone any other unidentified regions like them with $a > 2$ AU, were heavily populated early in Solar System history. This means we cannot completely rule out the possibility that the declining bombardment was produced by bodies that leaked out from refugia at the appropriate times to produce the Nectarian and early-Imbrium basins. With that said, the refugia populations would need size-frequency distributions and decay timescales that (i) produce basin sets A and B at the right times, (ii) avoid making lunar basins between 0–3.7 Ga, and (iii) avoid leaving behind a reservoir of small objects readily detected by small body surveys. Though we have yet to numerically model all of the possibilities, insights gleaned from this paper's results make us skeptical that any population residing in refugia could match these constraints.

As an example, consider the objects identified in our two long-lived niches. As stated above, there are 10 objects with absolute magnitude $15 < H < 19$ in the 0.6 Gy long-lived tail and 15 bodies with $14 < H < 16$ in the 1.2 Gy long-lived tail. For reference, an $H = 15$ NEO with a 14% albedo has a diameter of 3.5 km. Using the decay rates in Fig. 3, the 0.6 Gy tail has lost 0.06% of its population per My for the last several Gy, while the 1.2 Gy tail has lost 0.03% of its population per My for the last several Gy. Extrapolating these values back to 3.8 Ga, we find their initial populations were only 10–20 times as large as they

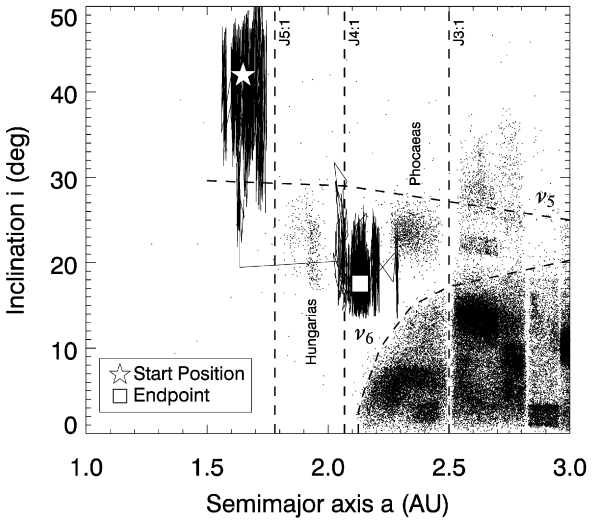

Fig. 10. A small portion of the dynamical evolution of a test body finding the long-lived niche described in Fig. 2. The black dots show the known asteroids of the inner Solar System with absolute magnitude $H < 15$. For reference, mean motion resonances with Jupiter (J3:1, J4:1, J5:1) and secular resonances (ν_5, ν_6) are shown as dotted lines. Planetary close encounters caused the body to move from an $a < 2$ AU orbit to an $a > 2$ AU orbit. The test body spends most of its time in a region between the stable Hungaria and Phocaea asteroid regions with orbital parameters $a = 2.13$–2.16 AU, $e = 0.16$–0.30, and $i = 17°$–$26°$.

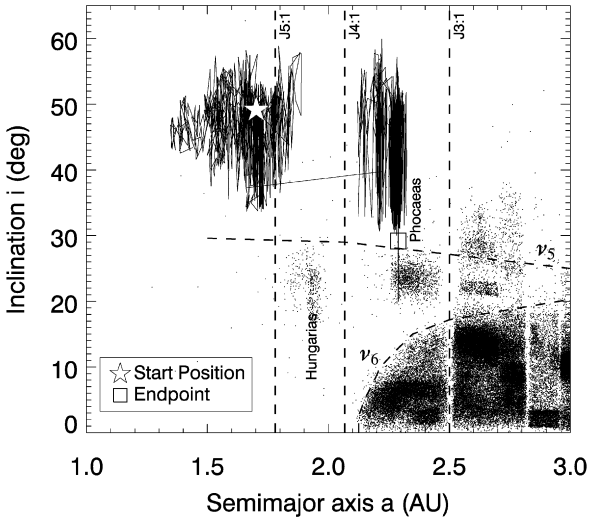

Fig. 11. A small portion of the dynamical evolution of a test body finding the second long-lived niche described in Fig. 3 (i.e., where the curve breaks away from the others at 1.2 Gy). The black dots show the known asteroids of the inner Solar System with $H < 15$. The star shows the starting orbit of this test body at the beginning of the sixth generation, while the square shows its orbit at the end of the sixth generation. Like the particle shown in Fig. 10, planetary close encounters caused the body to move from an $a < 2$ AU orbit to an $a > 2$ AU orbit. The body then settles in near the square and stays there for its remaining time. We characterize this region as having orbital parameters $a \approx 2.29$ AU, $e = 0.15$–0.30, and $i = 23°$–$30°$. This region also includes a resonance that intersects the Phocaea asteroid region.

are today. This translates into each niche having the order of 100 $D > 3.5$ km bodies at the time the early-Imbrium basins were produced. These values are far too small to expect the refugia-populations to produce the large numbers of $D > 64$ km objects needed to create basin sets A and B, particularly when one factors in the modest lunar collision probabilities shown in Fig. 4.

References

Agnor, C.B., Canup, R.M., Levison, H.F., 1999. On the character and consequences of large impacts in the late stage of terrestrial planet formation. Icarus 142, 219–237.

Agnor, C.B., Ward, W.R., 2002. Damping of terrestrial-planet eccentricities by density–wave interactions with a remnant gas disk. Astrophys. J. 567, 579–586.

Baldwin, R.B., 2006. Was there ever a terminal lunar cataclysm? Icarus 184, 308–318.

Baldwin, R.B., 1987a. On the relative and absolute ages of seven lunar front face basins. I. From viscosity arguments. Icarus 71, 1–18.

Baldwin, R.B., 1987b. On the relative and absolute ages of seven lunar front face basins. II. From crater counts. Icarus 71, 19–29.

Bernstein, G.M., Trilling, D.E., Allen, R.L., Brown, M.E., Holman, M., Malhotra, R., 2004. The size distribution of trans-neptunian bodies. Astron. J. 128, 1364–1390.

Bogard, D., 1995. Impact ages of meteorites: A synthesis. Meteoritics 30, 244–268.

Bottke, W.F., Greenberg, R., 1993. Asteroidal collision probabilities. Geophys. Res. Lett. 20, 879–881.

Bottke, W.F., Nolan, M.C., Greenberg, R., Kolvoord, R.A., 1994a. Velocity distributions among colliding asteroids. Icarus 107, 255–268.

Bottke, W.F., Nolan, M.C., Greenberg, R., Kolvoord, R.A., 1994b. Collisional lifetimes and impact statistics of near-Earth asteroids. In: Gehrels, T., Matthews, M.S. (Eds.), Hazards Due to Comets and Asteroids. Univ. of Arizona Press, Tucson, pp. 337–357.

Bottke, W.F., Jedicke, R., Morbidelli, A., Petit, J.-M., Gladman, B., 2000. Understanding the distribution of near-Earth asteroids. Science 288, 2190–2194.

Bottke, W.F., Morbidelli, A., Jedicke, R., Petit, J., Levison, H.F., Michel, P., Metcalfe, T.S., 2002. Debiased orbital and absolute magnitude distribution of the near-Earth objects. Icarus 156, 399–433.

Bottke, W.F., Durda, D., Nesvorny, D., Jedicke, R., Morbidelli, A., Vokrouhlicky, D., Levison, H., 2005a. The fossilized size distribution of the main asteroid belt. Icarus 175, 111–140.

Bottke, W.F., Morbidelli, A., Jedicke, R., Petit, J., Levison, H.F., Michel, P., Metcalfe, T.S., 2005b. Linking the collisional history of the main asteroid belt to its dynamical excitation and depletion. Icarus 179, 63–94.

Bottke, W.F., Nesvorný, D., Grimm, R.E., Morbidelli, A., O'Brien, D.P., 2006a. Iron meteorites as remnants of planetesimals formed in the terrestrial planet region. Nature 439, 821–824.

Bottke, W.F., Vokrouhlicky, D., Rubincam, D.P., Nesvorny, D., 2006b. The Yarkovsky and YORP effects: Implications for asteroid dynamics. Annu. Rev. Earth Planet. Sci. 34, 157–191.

Britt, D.T., Yeomans, D., Housen, K., Consolmagno, G., 2002. Asteroid density, porosity, and structure. In: Bottke, W.F., Cellino, A., Paolicchi, P., Binzel, R.P. (Eds.), Asteroids III. Univ. of Arizona Press, Tucson, pp. 485–500.

Buczkowski, D.L., Frey, H.V., Roark, J.H., McGill, G.E., 2005. Buried impact craters: A topographic analysis of quasi-circular depressions, Utopia Basin, Mars. J. Geophys. Res. 110. 3007.

Canup, R.M., 2004. Dynamics of lunar formation. Annu. Rev. Astron. Astrophys. 42, 441–475.

Campo Bagatin, A., Cellino, A., Davis, D.R., Farinella, P., Paolicchi, P., 1994. Wavy size distributions for collisional systems with a small-size cutoff. Planet. Space Sci. 42, 1079–1092.

Chambers, J., 2006. A semi-analytic model for oligarchic growth. Icarus 180, 496–513.

Chambers, J.E., 2001. Making more terrestrial planets. Icarus 152, 205–224.

Chambers, J.E., Cassen, P., 2002. The effects of nebula surface density profile and giant-planet eccentricities on planetary accretion in the inner Solar System. Meteor. Planet. Sci. 37, 1523–1540.

Chambers, J.E., Lissauer, J.J., 2002. A new dynamical model for the lunar Late Heavy Bombardment. Lunar Planet. Sci. 33. Abstract 1093.

Chambers, J.E., Wetherill, G.W., 1998. Making the terrestrial planets: N-body integrations of planetary embryos in three dimensions. Icarus 136, 304–327.

Chambers, J.E., Wetherill, G.W., 2001. Planets in the asteroid belt. Meteor. Planet. Sci. 36, 381–399.

Chapman, C.R., Cohen, B.A., Grinspoon, D.H., 2007. What are the real constraints on the existence and magnitude of the late heavy bombardment? Icarus, in press.

Cohen, B.A., 2002. Geochemical and geochronological constraints on early lunar bombardment history. Lunar Planet. Sci. 33. Abstract 1984.

Cohen, B.A., Swindle, T.D., Kring, D.A., 2000. Support for the lunar cataclysm hypothesis from lunar meteorite impact melt ages. Science 290, 1754–1756.

Cook, A.C., Watters, T.R., Robinson, M.S., Spudis, P.D., Bussey, D.B.J., 2000. Lunar polar topography derived from Clementine stereoimages. J. Geophys. Res. 105, 12023–12034.

Dalrymple, G.B., Ryder, G., 1993. ^{40}Ar–^{39}Ar age spectra of Apollo 15 impact melt rocks by laser step-heating and their bearing on the history of lunar basin formation. J. Geophys. Res. 98, 13085–13095.

Davis, D.R., Durda, D.D., Marzari, F., Campo Bagatin, A., Gil-Hutton, R., 2002. Collisional evolution of small body populations. In: Bottke, W.F., Cellino, A., Paolicchi, P., Binzel, R.P. (Eds.), Asteroids III. Univ. of Arizona Press, Tucson, pp. 545–558.

Dohnanyi, J.W., 1969. Collisional models of asteroids and their debris. J. Geophys. Res. 74, 2531–2554.

Durda, D.D., 1993. The collisional evolution of the asteroid belt and its contribution to the zodiacal cloud. Ph.D. thesis, Univ. of Florida.

Durda, D.D., Greenberg, R., Jedicke, R., 1998. Collisional models and scaling laws: A new interpretation of the shape of the main-belt asteroid size distribution. Icarus 135, 431–440.

Durda, D.D., Stern, S.A., Colwell, W.B., Parker, J.W., Levison, H.F., Hassler, D.M., 2000. A new observational search for vulcanoids in SOHO/LASCO coronagraph images. Icarus 148, 312–315.

Evans, N.W., Tabachnik, S., 1999. Possible long-lived asteroid belts in the inner Solar System. Nature 399, 41.

Evans, N.W., Tabachnik, S.A., 2002. Structure of possible long-lived asteroid belts. Mon. Not. R. Astron. Soc. 333, L1–L5.

Farinella, P., Davis, D.R., 1992. Collision rates and impact velocities in the main asteroid belt. Icarus 97, 111–123.

Frey, H.V., 2006. Impact constraints on the age and origin of the lowlands of Mars. Geophys. Res. Lett. 33. L08S02.

Frey, H.V., Roark, J.H., Shockey, K.M., Frey, E.L., Sakimoto, S.E.H., 2002. Ancient lowlands on Mars. Geophys. Res. Lett. 29. 1384.

Greenberg, R., 1982. Orbital interactions–A new geometrical formalism. Astron. J. 87, 184–195.

Greenberg, R., Hartmann, W.K., Chapman, C.R., Wacker, J.F., 1978. Planetesimals to planets—Numerical simulation of collisional evolution. Icarus 35, 1–26.

Gladman, B.J., Migliorini, F., Morbidelli, A., Zappalà, V., Michel, P., Cellino, A., Froeschlé, C., Levison, H.F., Bailey, M., Duncan, M., 1997. Dynamical lifetimes of objects injected into asteroid belt resonances. Science 277, 197–201.

Gnos, E., Hofmann, B.A., Al-Kathiri, A., Lorenzetti, S., Eugster, O., Whitehouse, M.J., Villa, I.M., Jull, A.J., Eikenberg, J., Spettel, B., Krähenbühl, U., Franchi, I.A., Greenwood, R.C., 2004. Pinpointing the source of a lunar meteorite: Implications for the Evolution of the Moon. Science 305, 657–659.

Grieve, R.A.F., Shoemaker, E.M., 1994. The record of past impacts on Earth. In: Gehrels, T., Matthews, M.S. (Eds.), Hazards Due to Comets and Asteroids. Univ. of Arizona Press, Tucson, pp. 417–462.

Grinspoon, D.H., 1989. Large impact events and atmospheric evolution on the terrestrial planets. Ph.D. thesis.

Goldreich, P., Ward, W.R., 1973. The formation of planetesimals. Astrophys. J. 183, 1051–1062.

Gomes, R., Levison, H.F., Tsiganis, K., Morbidelli, A., 2005. Origin of the cataclysmic Late Heavy Bombardment period of the terrestrial planets. Nature 435, 466–469.

Halliday, A.N., 2000. Terrestrial accretion rates and the origin of the Moon. Earth Planet. Sci. Lett. 176, 17–30.

Hartmann, W.K., 1975. Lunar 'cataclysm'—A misconception. Icarus 24, 181–187.

Hartmann, W.K., 1980. Dropping stones in magma oceans—Effects of early lunar cratering. In: Papike, J., Merrill, R. (Eds.), Conference on the Lunar Highlands Crust, Houston, Texas, November 14–16, 1979, Proceedings. Pergamon, New York, pp. 155–171.

Hartmann, W.K., 2003. Megaregolith evolution and cratering cataclysm models–Lunar cataclysm as a misconception (28 years later). Meteor. Planet. Sci. 38, 579–593.

Hartmann, W.K., Neukum, G., 2001. Cratering chronology and the evolution of Mars. Space Sci. Rev. 96, 165–194.

Hartmann, W.K., Strom, R.G., Grieve, R.A.F., Weidenschilling, S.J., Diaz, J., Blasius, K.R., Chapman, C.R., Woronow, A., Shoemaker, E.M., Dence, M.R., Jones, K.L., 1981. Chronology of planetary volcanism by comparative studies of planetary cratering. In: Basaltic Volcanism on the Terrestrial Planets, Basaltic Volcanism Study Project. Pergamon, New York, pp. 1048–1127. Full text at http://adsbit.harvard.edu/books/bvtp/.

Hartmann, W.K., Ryder, G., Dones, L., Grinspoon, D., 2000. The time-dependent intense bombardment of the primordial Earth/Moon system. In: Canup, R., Righter, K. (Eds.), Origin of the Earth and the Moon. Univ. of Arizona Press, Tucson, pp. 805–826.

Hartung, J.B., 1974. Can random impacts cause the observed AR 39/40 age distribution for lunar highland rocks? Meteoritics 9, 349.

Haskin, L.A., Korotev, R.L., Rockow, K.M., Jolliff, B.L., 1998. The case for an Imbrium origin of the Apollo Th-rich impact-melt breccias. Meteor. Planet. Sci. 33, 959–975.

Kenyon, S.J., Bromley, B.C., 2006. Terrestrial planet formation. I. The transition from oligarchic growth to chaotic growth. Astron. J. 131, 1837–1850.

Kleine, T., Münker, C., Mezger, K., Palme, H., 2002. Rapid accretion and early core formation on asteroids and the terrestrial planets from Hf-W chronometry. Nature 418, 952–955.

Korotev, R.L., Gillis, J.J., Haskin, L.A., Jolliff, B.L., 2002. On the Age of the Nectaris Basin. In: Lawrence, D.J., Duke, M.B. (Eds.), The Moon Beyond 2002: Next Steps in Lunar Science and Exploration, vol. 3029. The Lunar and Planetary Institute, Houston.

Kokubo, E., Ida, S., 2002. Formation of protoplanet systems and diversity of planetary systems. Astrophys. J. 581, 666–680.

Kokubo, E., Kominami, J., Ida, S., 2006. Formation of terrestrial planets from protoplanets. I. Statistics of basic dynamical properties. Astrophys. J. 642, 1131–1139.

Kominami, J., Ida, S., 2004. Formation of terrestrial planets in a dissipating gas disk with Jupiter and Saturn. Icarus 167, 231–243.

Kominami, J., Tanaka, H., Ida, S., 2005. Orbital evolution and accretion of protoplanets tidally interacting with a gas disk. Icarus 178, 540–552.

Kring, D.A., Cohen, B.A., 2002. Cataclysmic bombardment throughout the inner Solar System 3.9–4.0 Ga. J. Geophys. Res. 107. 4-1 to 4-6.

Leake, M.A., Chapman, C.R., Weidenschilling, S.J., Davis, D.R., Greenberg, R., 1987. The chronology of Mercury's geological and geophysical evolution—The vulcanoid hypothesis. Icarus 71, 350–375.

Lee, D.-C., Halliday, A.N., Snyder, G.A., Taylor, L.A., 1997. Age and origin of the Moon. Science 278, 1098.

Levison, H.F., Agnor, C., 2003. The role of giant planets in terrestrial planet formation. Astron. J. 125, 2692–2713.

Levison, H.F., Duncan, M.J., 1994. The long-term dynamical behavior of short-period comets. Icarus 108, 18–36.

Levison, H.F., Dones, L., Chapman, C.R., Stern, S.A., Duncan, M.J., Zahnle, K., 2001. Could the lunar "Late Heavy Bombardment" have been triggered by the formation of Uranus and Neptune? Icarus 151, 286–306.

Levison, H.F., Thommes, E., Duncan, M.J., Dones, L., 2004. A fairy tale about the formation of Uranus and Neptune and the lunar Late Heavy Bombardment. In: Debris Disks and the Formation of Planets. In: ASP Conf. Ser., vol. 324, p. 152.

Levison, H., Nesvorny, D., Agnor, C., Morbidelli, A., 2005. The role of dynamical friction in terrestrial planet formation. Bull. Am. Astron. Soc. 37. Abstracts 25.01.

Marzari, F., Scholl, H., Murray, C., Lagerkvist, C., 2002. Origin and evolution of trojan asteroids. In: Bottke, W.F., Cellino, A., Paolicchi, P., Binzel, R.P. (Eds.), Asteroids III. Univ. of Arizona Press, Tucson, pp. 725–738.

McEwen, A.S., Moore, J.M., Shoemaker, E.M., 1997. The Phanerozoic impact cratering rate: Evidence from the farside of the Moon. J. Geophys. Res. 102, 9231–9242.

McEwen, A.S., Gaddis, L.R., Neukum, G., Hoffmann, H., Pieters, C.M., Head, J.W., 1993. Galileo observations of post-imbrium lunar craters during the first Earth–Moon flyby. J. Geophys. Res. 98, 17207–17234.

McNeil, D., Duncan, M., Levison, H.F., 2005. Effects of type I migration on terrestrial planet formation. Astron. J. 130, 2884–2899.

Michel, P., Migliorini, F., Morbidelli, A., Zappalà, V., 2000. The population of Mars-crossers: Classification and dynamical evolution. Icarus 145, 332–347.

Michel, P., 1998. Dynamical behavior of near-Earth asteroids in the terrestrial planet region: The role of secular resonances. Planet. Space Sci. 46, 905–910.

Migliorini, F., Michel, P., Morbidelli, A., Nesvorný, D., Zappalà, V., 1998. Origin of Earth crossing asteroids: A quantitative simulation. Science 281, 2022–2024.

Morbidelli, A., Petit, J.-M., Gladman, B., Chambers, J., 2001. A plausible cause of the late heavy bombardment. Meteor. Planet. Sci. 36, 371–380.

Morbidelli, A., Levison, H.F., Tsiganis, K., Gomes, R., 2005. Chaotic capture of Jupiter's Trojan asteroids in the early Solar System. Nature 435, 462–465.

Neukum, G., 1977. Different ages of lunar light plains. Moon 17, 383–393.

Neukum, G., Ivanov, B.A., 1994. Crater size distributions and impact probabilities on Earth from lunar, terrestrial-planet, and asteroid cratering data. In: Gehrels, T., Matthews, M.S. (Eds.), Hazards Due to Comets and Asteroids. Univ. of Arizona Press, Tucson, pp. 359–416.

Neukum, G., Ivanov, B.A., Hartmann, W.K., 2001a. Cratering records in the inner Solar System in relation to the lunar reference system. Space Sci. Rev. 96, 55–86.

Neukum, G., Oberst, J., Hoffmann, H., Wagner, R., Ivanov, B.A., 2001b. Geologic evolution and cratering history of Mercury. Planet. Space Sci. 49, 1507–1521.

Norman, M.D., Taylor, L.A., 2005. Testing the lunar cataclysm: Identification of lunar impact melts possibly older than Nectaris. Lunar Planet. Sci. 36. Abstract 1570.

Norman, M.D., Duncan, R.A., Huard, J.J., 2006. Identifying impact events within the lunar cataclysm from ^{40}Ar–^{39}Ar ages and compositions of Apollo 16 impact melt rocks. Geochim. Cosmochim. Acta 70, 6032–6049.

Norman, M.D., Borg, L.E., Nyquist, L.E., Bogard, D.D., 2003. Chronology, geochemistry, and petrology of a ferroan noritic anorthosite clast from Descartes breccia 67215: Clues to the age, origin, structure, and impact history of the lunar crust. Meteor. Planet. Sci. 38, 645–661.

O'Brien, D.P., Greenberg, R., 2003. Steady-state size distributions for collisional populations: Analytical solution with size-dependent strength. Icarus 164, 334–345.

O'Brien, D.P., Morbidelli, A., Bottke, W.F., 2005. Collisional evolution of the primordial trans-neptunian disk: Implications for planetary migration and the current size distribution of TNOs. Bull. Am. Astron. Soc. 37, 676.

O'Brien, D.P., Morbidelli, A., Levison, H.F., 2006. Terrestrial planet formation with strong dynamical friction. Icarus 184, 39–58.

Opik, E.J., 1951. Collision probability with the planets and the distribution of planetary matter. Proc. R. Irish Acad. 54, 165–199.

Petit, J., Morbidelli, A., Chambers, J., 2001. The primordial excitation and clearing of the asteroid belt. Icarus 153, 338–347.

Raymond, S.N., Quinn, T., Lunine, J.I., 2006. High-resolution simulations of the final assembly of Earth-like planets. I. Terrestrial accretion and dynamics. Icarus 183, 265–282.

Raymond, S.N., Quinn, T., Lunine, J.I., 2004. Making other Earths: Dynamical simulations of terrestrial planet formation and water delivery. Icarus 168, 1–17.

Ryder, G., Koeberl, C., Mojzsis, S.J., 2000. Heavy bombardment on the Earth at 3.85 Ga: The search for petrographic and geochemical evidence. In: Canup,

R.M., Righter, K. (Eds.), Origin of the Earth and Moon. Univ. of Arizona Press, Tucson, pp. 475–492.

Segura, T.L., Toon, O.B., Colaprete, A., Zahnle, K., 2002. Environmental effects of large impacts on Mars. Science 298, 1977–1980.

Shukolyukov, A., Lugmair, G.W., 2002. Chronology of asteroid accretion and differentiation. In: Bottke, W.F., Cellino, A., Paolicchi, P., Binzel, R.P. (Eds.), Asteroids III. University of Arizona Press, Tucson, pp. 687–695.

Shoemaker, E.M., Shoemaker, C.S., 1996. The Proterozoic impact record in Australia. AGSO J. Aust. Geol. Geophys. 16, 379–398.

Shoemaker, E.M., 1998. Long term variations in the impact cratering rate on Earth. In: Grady, M., Hutchison, R., McCall, G.J.H., Rothery, D.A. (Eds.), Meteorites: Flux with Time and Impact Effects. In: Special Publications, vol. 140. Geological Society, London, pp. 7–10.

Smith, D.E., Zuber, M.T., Neumann, G.A., Lemoine, F.G., 1997. Topography of the Moon from the Clementine lidar. J. Geophys. Res. 102, 1591–1611.

Stern, S.A., Durda, D.D., 2000. Collisional evolution in the vulcanoid region: Implications for present-day population constraints. Icarus 143, 360–370.

Stern, S.A., Levison, H.F., 1999. A warm early Mars and CO_2 influx from the Late Heavy Bombardment. Lunar Planet. Sci. 30. Abstracts 1141.

Stöffler, D., Ryder, G., 2001. Stratigraphy and isotope ages of lunar geologic units: Chronological standard for the inner Solar System. Space Sci. Rev. 96, 9–54.

Strom, R.G., Neukum, G., 1988. The cratering record on Mercury and the origin of impacting objects. In: Vilas, F., Chapman, C.R., Matthews, M.S. (Eds.), Mercury. Univ. of Arizona Press, Tucson, pp. 336–373.

Strom, R.G., Croft, S.K., Barlow, N.G., 1992. The martian impact cratering record. In: Kieffer, H.H., Jakosky, B.M., Snyder, C.W., Matthews, M.S. (Eds.), Mars. Univ. of Arizona Press, Tucson, pp. 383–423.

Strom, R.G., Malhotra, R., Ito, T., Yoshida, F., Kring, D.A., 2005. The origin of planetary impactors in the inner Solar System. Science 309, 1847–1850.

Tagle, R., 2005. LL-ordinary chondrite impact on the Moon: Results from the 3.9 Ga impact melt at the landing site of Apollo 17. Lunar Planet. Sci. 36. 2008.

Tanga, P., Weidenschilling, S.J., Michel, P., Richardson, D.C., 2004. Gravitational instability and clustering in a disk of planetesimals. Astron. Astrophys. 427, 1105–1115.

Taylor, G.J., 1998. The biggest hole in the Solar System. Planetary Science Research Discoveries. http://www.psrd.hawaii.edu/July98/spa.html. Posted on July 17, 1998.

Tera, F., Papanastassiou, D.A., Wasserburg, G.J., 1974. Isotopic evidence for a terminal lunar cataclysm. Earth Planet. Sci. Lett. 22, 1–21.

Touma, J., Wisdom, J., 1994. Evolution of the Earth–Moon system. Astron. J. 108, 1943–1961.

Trail, D., Mojzsis, S.J., Harrison, T.M., Levison, H.F., 2007. Do Hadean zircons retain a record of the Late Heavy Bombardment on Earth? Geochim. Cosmochimi. Acta, in press.

Tsiganis, K., Gomes, R., Morbidelli, A., Levison, H.F., 2005. Origin of the orbital architecture of the giant planets of the Solar System. Nature 435, 459–461.

Vokrouhlický, D., Farinella, P., Bottke, W.F., 2000. The depletion of the putative vulcanoid population via the Yarkovsky effect. Icarus 148, 147–152.

Ward, W.R., Canup, R.M., 2000. Origin of the Moon's orbital inclination from resonant disk interactions. Nature 403, 741–743.

Warren, P.H., 2003. Lunar prospector data imply an age of 4.1 Ga for the Nectaris Basin, and other problems with the lunar "Cataclysm" hypothesis. In: Large Meteorite Impacts Conference, p. 4129.

Warren, P.H., 2004. The Moon. In: Holland, H.D., Turekian, K.K. (Eds.), Treatise on Geochemistry. Elsevier, Amsterdam, pp. 559–599.

Weidenschilling, S.J., 1977. The distribution of mass in the planetary system and solar nebula. Astrophys. Space Sci. 51, 153–158.

Weidenschilling, S.J., 2003. Radial drift of particles in the solar nebula: Implications for planetesimal formation. Icarus 165, 438–442.

Weidenschilling, S.J., Spaute, D., Davis, D.R., Marzari, F., Ohtsuki, K., 1997. Accretional evolution of a planetesimal swarm. Icarus 128, 429–455.

Wetherill, G.W., 1967. Collisions in the asteroid belt. J. Geophys. Res. 72, 2429–2444.

Wetherill, G.W., 1975. Late heavy bombardment of the moon and terrestrial planets. Proc. Lunar Sci. Conf. 6, 1539–1561.

Wetherill, G.W., 1977. Evolution of the Earth's planetesimal swarm subsequent to the formation of the Earth and Moon. Proc. Lunar Sci. Conf. 8, 1–16.

Wetherill, G.W., 1992. An alternative model for the formation of the asteroids. Icarus 100, 307–325.

Wetherill, G.W., Stewart, G.R., 1989. Accumulation of a swarm of small planetesimals. Icarus 77, 330–357.

Wilhelms, D.E., 1987. The Geologic History of the Moon. US Geol. Surv. Prof. Pap. 1348, 302 pp. (full text at http://ser.sese.asu.edu/GHM/).

Wisdom, J., Holman, M., 1991. Symplectic maps for the N-body problem. Astron. J. 102, 1528–1538.

Wood, C., 2004. Impact basin database. http://www.lpod.org/cwm/DataStuff/Lunar%20Basins.htm.

Youdin, A.N., Goodman, J., 2005. Streaming instabilities in protoplanetary disks. Astrophys. J. 620, 459–469.

Youdin, A.N., Chiang, E.I., 2004. Particle pileups and planetesimal formation. Astrophys. J. 601, 1109–1119.

Zahnle, K.J., Sleep, N.H., 1997. Impacts and the early evolution of life. In: Thomas, P.J., Chyba, C.F., McKay, C.P. (Eds.), Comets and the Origin and Evolution of Life. Springer-Verlag, New York, pp. 175–208.